Applied Mathematics and Computation 234 (2014) 557–578

Contents lists available at ScienceDirect

Applied Mathematics and Computation

journal homepage: www.elsevier.com/locate/amc

A nonlocal meshless solution for flexural vibrations of double-walled carbon nanotubes

Keivan Kiani

Department of Civil Engineering, K.N. Toosi University of Technology, Tehran, Iran

ARTICLE INFO

Keywords:
Free transverse vibration
Vibration mode shapes
Double-walled carbon nanotubes (DWCNTs)
Nonlocal Rayleigh beam theory
Reproducing kernel particle method (RKPM)

ABSTRACT

The true understanding of free vibration of double-walled carbon nanotubes (DWCNTs) plays a vital role in optimal design and dynamic control of such nanostructures. This paper is aimed to examine free flexural vibration of lengthy DWCNTs with arbitrary boundary conditions in the framework of nonlocal elasticity theory. The DWCNTs are embedded in an elastic medium and are subjected to initially axial forces. Equivalent continuum structures associated with the innermost and outermost tubes of the DWCNT are considered. The transverse and rotational interactions of the DWCNT with the surrounding elastic medium are also taken into account. The generalized equations of motion of lengthy DWCNTs are established based on the nonlocal Rayleigh beam theory. Seeking an analytical solution to the developed equations, particularly in their general form, is a very problematic task. As an alternative solution, an efficient numerical scheme is proposed. The effects of slenderness ratio, small-scale parameter, lateral and rotational stiffness of the surrounding matrix, and initially axial force on the first five natural frequencies of DWCNTs under different boundary conditions are comprehensively scrutinized.

1. Introduction

The discovery of carbon nanotubes (CNTs) has opened up a new world in the field of nanotechnology. Since the past three decades, four major forms of carbon materials have come to the real world; those are C_{60} by Kroto et al. [1] in 1985, multi-walled carbon nanotube (MWCNT) by Iijima [2] in 1991, single-walled carbon nanotube (SWCNT) by Bethune et al. [3] in 1993, and carbon nanofiber. Subsequent studies revealed that CNTs integrate astonishing rigid and toughness properties, such as exceptionally high elastic properties, huge elastic strain, and fracture strain sustaining capability [4–8]. Beyond any exaggeration, CNTs are the strongest fibers recognized to date. The Young's modulus of a SWCNT is around 1 TPa, which is five times greater than steel, while its density is only 1200–1400 kg/m^3 [9]. It implies that the macro-scale structures made of CNTs will be extremely lighter and stronger than steel frames. Further studies reported that the frequency of flexural vibration of CNTs could reach the level of GHz [10,11] or even THz [12]. These evidences indicate that CNTs could be regarded as the most capable reinforcement materials for the next generation of high frequency engineered structures. Thereby, they have attracted the attention of both engineering and scientific communities of various disciplines during recent years. As a result, understanding the true mechanisms of their vibrations under various boundary conditions would be of great advantageous in optimal design of such nanostructures as well as future macro-scale structures made of CNTs.

Generally, free vibration of MWCNTs can be explored by using an atomistic-based approach, a classical continuum-based model, or via a nonlocal continuum-based model. In the two later models, numerical schemes or analytical solutions may be

E-mail addresses: k_kiani@kntu.ac.ir, keivankiani@yahoo.com

http://dx.doi.org/10.1016/j.amc.2014.01.015
0096-3003/

implemented for solving the governing equations. The choice of the model in any circumstance entails a tradeoff in that. For example, atomistic-based models commonly lead to more accurate results. However, they are really time-consuming and labor intensive, which is not the case for the models based on the classical or even the nonlocal continuum mechanics. In the continuum-based models, the CNT is treated as a continuous material with specific geometry and elastic materials' properties. The classical continuum models which are used for flexural vibration of DWCNTs or MWCNTs are commonly based on the traditional engineering models such as beams [13–24] and shells [25–27]. The major drawback of such models is that the length of the C–C bond is not included in their formulations. This matter becomes highlighted particularly when the length of the nanostructure would be comparable with the length of the C–C bond or even when the wavelength of the propagated sound wave is fairly as small as the length of the C–C bonds. In order to conquer such a shortcoming of the classical models, other sophisticated continuum-based theories have been developed during the past century such as couple stress theory [28], modified couple stress theory [29,30], nonlocal continuum theory [31,32], and higher gradient continuum theory [33]. A simple version of the nonlocal continuum theory of Eringen [31,32] is the most popular one among the nanotechnologist since it could be readily applied to the classical governing equations. In this fairly novel theory, the lengths of interatomic bonds are incorporated into the equations of motion via a so-called small-scale parameter. For exploring flexural vibration of CNTs, an investigation by Duan et al. [34] revealed that the value of the small-scale parameter to use generally relies on the length-to-diameter ratios, mode shapes, and boundary conditions of the SWCNT. For each problem, the value of the small-scale parameter can be appropriately selected through justification of the predicted dispersion curves by the nonlocal model with those of an atomistic-based approach. Conversely, it seems that further research works are still needed to investigate the feasibility of application of other non-classical theories to free vibration of nanostructures. To date, nonlocal beam models [35–40] and nonlocal shells models [41,42] have been exploited for studying wave propagation within DWCNTs as well as flexural vibration of DWCNTs. In the present work, a nonlocal beam model is employed since only flexural vibration of DWCNTs is of particular interest. Among the beam theories, the Rayleigh beam theory is implemented since the understudy DWCNT is a lengthy nanostructure, and it is expected that the ratio of the shear strain energy to the flexural one would be negligible. Unlike the Euler–Bernoulli beam model, the rotary inertial of the DWCNT is also taken into account by the Rayleigh beam theory.

A brief survey of the literature displays that the research works on the vibration of DWCNTs in the context of nonlocal continuum theory of Eringen are limited to particular cases. For example, most of the previously published works were devoted to study free flexural vibration of simply supported DWCNTs [35,37,39] or flexural vibration of simply supported DWCNTs under external loads [43,44]. The main reason of this fact is that finding an analytical solution to the nonlocal governing equations pertinent to linear free flexural vibration of DWCNTs which are embedded in an elastic medium under arbitrary boundary conditions as well as initially axial forces is a very problematic task. To conquest such a dilemma, efficient numerical schemes could be implemented. In this work, reproducing kernel particle method (RKPM) is employed for solving the nonlocal equations of motion of lengthy DWCNTs. RKPM is an efficient meshless technique which is initially developed by Liu et al. [45]. To date, this method has been successfully applied to various engineering problems [46–49]. In contrast to finite element method (FEM), RKPM employs higher-order shape functions (i.e., interpolants) according to the used base function and window function. In FEM analysis, node-based meshes are used for discretizing of the spatial domain while in RKPM analysis, particles are used for this purpose. This matter provides RKPM for a wide class of continuum mechanics' problems, especially those undergoing mesh distortion, moving boundaries, higher gradients as well as those with higher-order derivatives. In the present work, the fourth derivatives of the deflection fields of the innermost and outermost tubes of the DWCNT appear in the equations of motion and it is anticipated that RKPM could reproduce the near to exact values of such deflection fields by using its higher-order interpolant shape functions.

Recently, Kiani [50] examined free transverse vibration of an embedded single-walled tube structure under different boundary conditions. Using various nonlocal beam models and RKPM inerpolants, the flexural frequencies of the nanostructure were obtained and the capabilities of the proposed models in capturing the flexural frequencies of the nanostructure were also studied.

In this article, flexural vibration characterization of a lengthy DWCNT under arbitrary conditions is of concern. The DWCNT is subjected to an initially axial force and is embedded in an elastic matrix. Using Hamilton's principle, the dimensionless equations of motion of the considered DWCNTs are established on the basis of the Rayleigh's beam theory as well as nonlocal continuum theory of Eringen. Since finding an analytical solution to the governing equations is a very difficult task, an efficient meshless technique is proposed. The deflection fields of the innermost and outermost tubes of the lengthy DWCNT are discretized via RKPM, and the governing equations are reconstructed in the matrix form. In some special cases, the obtained results are also compared with those of other works. The roles of the influential parameters on the first five flexural frequencies of lengthy DWCNTs under different boundary conditions are explained and discussed in some detail.

2. Model description

Consider a lengthy elastically supported DWCNT embedded in an elastic medium. A schematic representation of the nanostructure has been shown in Fig. 1. The innermost and outermost tubes are modeled via equivalent continuum structures (ECSs). The ECS is a tubular structure whose length and most of its frequencies are identical to those of the original tube. The mean radius, walls' thickness, length, cross-sectional area, elasticity modulus, and density of the ECS associated

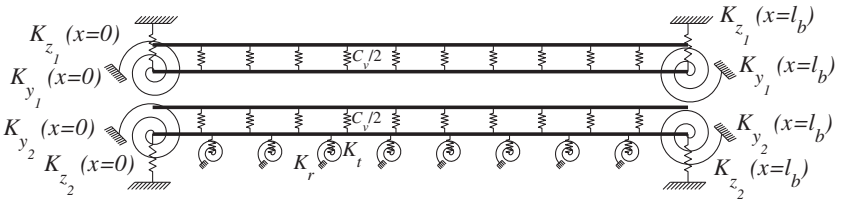

Fig. 1. Schematic representation of a lengthy elastically supported DWCNT embedded in an elastic medium.

with the innermost/outermost tube are represented by $r_{m_1}/r_{m_2}, t_{b_1}/t_{b_2}$, $l_b/l_b, A_{b_1}/A_{b_2}, E_{b_1}/E_{b_2}$, and ρ_{b_1}/ρ_{b_2}, respectively. The van der Waals interaction forces between the atoms of the innermost and outermost tubes are simulated by a continuous lateral spring system connecting two tubes. The stiffness of this spring system is denoted by C_v. For a lengthy DWNCT, its value can be calculated based on Ref. [53,43]. The initially axial forces within the innermost and outermost tubes in order are represented by N_{b_1} and N_{b_2}. The interaction of the DWCNT with its surrounding matrix is modeled by an elastic layer consisting of continuous lateral and rotary springs with constants K_t and K_r, respectively. Additionally, both ends of the ECSs have been attached to lateral and rotary springs with constants K_{z_i} and K_{y_i}, respectively (see Fig. 1). The choice of the levels of these constants enables us to study free flexural vibration of a lengthy DWCNT for a wide range of boundary conditions.

In the next part, for assessing free dynamic analysis of the two linked ECSs, Rayleigh beam theory (RBT) is employed. The small-scale parameter is also incorporated into the formulations of the problem using nonlocal continuum theory of Eringen. Subsequently, the equations of motion describing the lateral vibration of a lengthy elastically supported DWCNT embedded in an elastic matrix are obtained.

3. Transverse vibration DWCNTs via a nonlocal continuum-based beam theory

3.1. Nonlocal equations of motion of DWCNTs

Based on the NRBT, the kinetic energy, $T(t)$, and the elastic strain energy, $U(t)$, of an elastically supported DWCNT embedded in an elastic medium are expressed by:

$$\begin{aligned} T(t) &= \frac{1}{2}\sum_{i=1}^{2}\int_0^{l_b}\rho_{b_i}\left(A_{b_i}(\dot{w}_i(x,t))^2 + I_{b_i}(\dot{w}_{i,x}(x,t))^2\right)dx,\\ U(t) &= \frac{1}{2}\sum_{i=1}^{2}\int_0^{l_b}\left(-w_{i,xx}(x,t)M_{b_i}^{nl}(x,t) + N_{b_i}(w_{i,x}(x,t))^2\right)dx + \frac{1}{2}\int_0^{l_b}C_v(w_2(x,t)-w_1(x,t))^2\,dx\\ &\quad + \frac{1}{2}\int_0^{l_b}\left(K_t(w_2(x,t))^2 + K_r(w_{2,x}(x,t))^2\right)dx + \frac{1}{2}\sum_{i=1}^{2}\sum_{k=1}^{2}\left(K_{z_i}(x_k)(w_i(x_k,t))^2 + K_{y_i}(x_k)(w_{i,x}(x_k,t))^2\right), \end{aligned} \tag{1}$$

where $w_1(x,t)/M_{b_1}^{nl}(x,t)$ and $w_2(x,t)/M_{b_2}^{nl}(x,t)$ denote the deflection/nonlocal bending moment fields of the innermost and outermost tubes, respectively. According to the nonlocal continuum theory of Eringen [31,32], the nonlocal bending moments of the inner and outer tubes which are modeled based on the NRBT are provided by [36,37,51,52]:

$$M_{b_i}^{nl} - (e_0a)^2M_{b_i,xx}^{nl} = -E_{b_i}I_{b_i}w_{i,xx};\quad i=1,2 \tag{2}$$

where a is an internal characteristic length. The value of e_0 is determined by adjusting the dispersion curves of the nonlocal model with those of another atomistic-based model when the experimentally observed data are not available. The parameter e_0a is called small-scale effect parameter or small-scale parameter. Using Hamilton's principle, $\int_0^t(\delta T(t)-\delta U(t))\,dt=0$, the strong form of the equations of motion characterizing the transverse vibration of DWCNTs embedded in an elastic matrix is obtained as:

$$\rho_{b_1}(A_{b_1}\ddot{w}_1 - I_{b_1}\ddot{w}_{1,xx}) - M_{b_1,xx}^{nl} + C_v(w_1-w_2) - (N_{b_1}w_{1,x})_{,x} + \sum_{k=1}^{2}(K_{z_1}(x_k)w_1 - K_{y_1}(x_k)w_{1,xx})\delta(x-x_k) = 0, \tag{3a}$$

$$\rho_{b_2}(A_{b_2}\ddot{w}_2 - I_{b_2}\ddot{w}_{2,xx}) - M_{b_2,xx}^{nl} - C_v(w_1-w_2) - (N_{b_2}w_{2,x})_{,x} + K_tw_2 - K_rw_{2,xx} + \sum_{k=1}^{2}(K_{z_2}(x_k)w_2 - K_{y_2}(x_k)w_{2,xx})\delta(x-x_k) = 0, \tag{3b}$$

where δ represents the Dirac delta function. By combining Eq. (2) with Eqs. (3a) and (3b), the nonlocal equations of motion for transverse vibration of DWCNTs in terms of deflection fields of the innermost and outermost tubes are obtained as follows:

$$\rho_{b_1}A_{b_1}\left(\ddot{w}_1-(e_0a)^2\ddot{w}_{1,xx}\right)-\rho_{b_1}I_{b_1}\left(\ddot{w}_{1,xx}-(e_0a)^2\ddot{w}_{1,xxxx}\right)+C_v\left(w_1-w_2-(e_0a)^2(w_{1,xx}-w_{2,xx})\right)$$
$$+E_{b_1}I_{b_1}w_{1,xxxx}-N_{b_1}\left(\ddot{w}_{1,xx}-(e_0a)^2\ddot{w}_{1,xxxx}\right)+\sum_{k=1}^{2}\Big(K_{z_1}(x_k)\left(w_1\delta(x-x_k)-(e_0a)^2(w_1\delta(x-x_k))_{,xx}\right)$$
$$-K_{y_1}(x_k)\left(w_{1,xx}\delta(x-x_k)-(e_0a)^2(w_{1,xx}\delta(x-x_k))_{,xx}\right)\Big)=0, \tag{4a}$$

$$\rho_{b_2}A_{b_2}\left(\ddot{w}_2-(e_0a)^2\ddot{w}_{2,xx}\right)-\rho_{b_2}I_{b_2}\left(\ddot{w}_{2,xx}-(e_0a)^2\ddot{w}_{2,xxxx}\right)-C_v\left(w_1-w_2-(e_0a)^2(w_{1,xx}-w_{2,xx})\right)$$
$$+E_{b_2}I_{b_2}w_{2,xxxx}-N_{b_2}\left(\ddot{w}_{2,xx}-(e_0a)^2\ddot{w}_{2,xxxx}\right)+K_t\left(w_2-(e_0a)^2w_{2,xx}\right)-K_r\left(w_{2,xx}-(e_0a)^2w_{2,xxxx}\right)$$
$$+\sum_{k=1}^{2}\Big(K_{z_2}(x_k)\left(w_2\delta(x-x_k)-(e_0a)^2(w_2\delta(x-x_k))_{,xx}\right)-K_{y_2}(x_k)\left(w_{2,xx}\delta(x-x_k)-(e_0a)^2(w_{2,xx}\delta(x-x_k))_{,xx}\right)\Big)=0. \tag{4b}$$

For examining the problem in a more general framework, the following dimensionless parameters are introduced:

$$\xi=\frac{x}{l_b},\quad \overline{w}_1=\frac{w_1}{l_b},\quad \overline{w}_2=\frac{w_2}{l_b},\quad \tau=\frac{1}{l_b^2}\sqrt{\frac{E_{b_1}I_{b_1}}{\rho_{b_1}A_{b_1}}}t,\quad \mu=\frac{e_0a}{l_b},\quad \lambda_1=\frac{l_b}{r_{b_1}}, \tag{5}$$

where ξ is the dimensionless coordinate, $\overline{w}_i$ is the dimensionless deflection field of the ith nanotube, τ is the dimensionless time parameter, μ is the dimensionless small-scale parameter, r_{b_1} denotes the gyration radius of the innermost tube, and λ_1 is the slenderness ratio of the innermost tube. Using Eqs. (4a), (4b), and (5), the dimensionless equations of motion are derived as follows:

$$\overline{w}_{1,\tau\tau}-\mu^2\overline{w}_{1,\tau\tau\xi\xi}-\lambda_1^{-2}\left(\overline{w}_{1,\tau\tau\xi\xi}-\mu^2\overline{w}_{1,\tau\tau\xi\xi\xi\xi}\right)+\overline{C}_v\left(\overline{w}_1-\overline{w}_2-\mu^2(\overline{w}_{1,\xi\xi}-\overline{w}_{2,\xi\xi})\right)+\overline{w}_{1,\xi\xi\xi\xi}-\overline{N}_{b_1}\left(\overline{w}_{1,\xi\xi}-\mu^2\overline{w}_{1,\xi\xi\xi\xi}\right)$$
$$+\sum_{k=1}^{2}\Big(\overline{K}_{z_1}(\xi_k)\left(\overline{w}_1\delta(\xi-\xi_k)-\mu^2(\overline{w}_1\delta(\xi-\xi_k))_{,\xi\xi}\right)-\overline{K}_{y_1}(\xi_k)\left(\overline{w}_{1,\xi\xi}\delta(\xi-\xi_k)-\mu^2(\overline{w}_{1,\xi\xi}\delta(\xi-\xi_k))_{,\xi\xi}\right)\Big)=0, \tag{6a}$$

$$\varrho_1^2\left(\overline{w}_{2,\tau\tau}-\mu^2\overline{w}_{2,\tau\tau\xi\xi}\right)-\varrho_2^2\lambda_1^{-2}\left(\overline{w}_{2,\tau\tau\xi\xi}-\mu^2\overline{w}_{2,\tau\tau\xi\xi\xi\xi}\right)-\overline{C}_v\left(\overline{w}_1-\overline{w}_2-\mu^2(\overline{w}_{1,\xi\xi}-\overline{w}_{2,\xi\xi})\right)$$
$$+\varrho_3^2\overline{w}_{2,\xi\xi\xi\xi}-\overline{N}_{b_2}\left(\overline{w}_{2,\xi\xi}-\mu^2\overline{w}_{2,\xi\xi\xi\xi}\right)+\overline{K}_t(\overline{w}_2-\mu^2\overline{w}_{2,\xi\xi})-\overline{K}_r(\overline{w}_{2,\xi\xi}-\mu^2\overline{w}_{2,\xi\xi\xi\xi})$$
$$+\sum_{k=1}^{2}\Big(\overline{K}_{z_2}(\xi_k)\left(\overline{w}_2\delta(\xi-\xi_k)-\mu^2(\overline{w}_2\delta(\xi-\xi_k))_{,\xi\xi}\right)-\overline{K}_{y_2}(\xi_k)\left(\overline{w}_{2,\xi\xi}\delta(\xi-\xi_k)-\mu^2(\overline{w}_{2,\xi\xi}\delta(\xi-\xi_k))_{,\xi\xi}\right)\Big)=0, \tag{6b}$$

where

$$\varrho_1^2=\frac{\rho_{b_2}A_{b_2}}{\rho_{b_1}A_{b_1}},\quad \varrho_2^2=\frac{\rho_{b_2}I_{b_2}}{\rho_{b_1}I_{b_1}},\quad \varrho_3^2=\frac{E_{b_2}I_{b_2}}{E_{b_1}I_{b_1}},\quad \overline{C}_v=\frac{C_vl_b^4}{E_{b_1}I_{b_1}},\quad \overline{N}_{b_i}=\frac{N_{b_i}l_b^2}{E_{b_1}I_{b_1}},$$
$$\overline{K}_{z_i}(\xi_k)=\frac{K_{z_i}(x_k)l_b^3}{E_{b_1}I_{b_1}},\quad \overline{K}_{y_i}(\xi_k)=\frac{K_{y_i}(x_k)l_b}{E_{b_1}I_{b_1}},\quad \overline{K}_t=\frac{K_tl_b^4}{E_{b_1}I_{b_1}},\quad \overline{K}_r=\frac{K_rl_b^2}{E_{b_1}I_{b_1}};\quad i,k=1,2, \tag{7}$$

Eqs. (6a) and (6b) furnish us with the strong form of the dimensionless equations of motion of an elastically supported DWCNT with initially axial force embedded in an elastic medium. Generally, finding an analytical solution to Eqs. (6a) and (6b) is a very difficult job. The analytical solutions to these equations are available just for particular cases. For instance, Yoon et al. [14] explored free flexural vibration of MWCNTs embedded in an elastic matrix in the framework of classical continuum theory (i.e., $\mu=0$). The ECSs associated with the innermost and outermost tubes of the DWCNT are modeled based on the Euler–Bernoulli beam theory. Their investigations were limited to the case of DWCNTs with clamped ends and only lateral interaction of the DWCNT with its surrounding matrix was taken into account. Based on the Euler–Bernoulli beam theory, Zhang et al. [15] proposed a double-elastic beam model for transverse vibrations of DWCNTs under compressive axial load. The governing equations of the proposed model were constructed in the context of classical continuum theory. Without considering the interaction of the DWCNT with its surrounding medium, the explicit expressions of flexural frequencies and associated amplitude ratios of the inner tube to the outer one were derived in the case of simply supported DWCNTs. Using Euler–Bernoulli beam model, Natsuki et al. [20] investigated the free flexural dynamic response of DWCNTs on the basis of the classical continuum theory. The considered DWCNT did not experience any initial axial force and it was released from the surrounding matrix. Moreover, free transverse vibrations of only simply supported DWCNTs were of concern. In the absence of surrounding elastic medium as well as initially axial forces, Zhang et al. [35] studied free transverse vibrations of DWCNTs based on the nonlocal Euler–Bernoulli beam theory. The frequency analyses of DWCNTs were carried out in the case of simply supported boundary conditions using eigen function expansion.

As it is seen in the literature, the undertaken works were restricted to some special boundary conditions. Moreover, the full interactions of DWCNTs with its surrounding matrix were not considered. In order to bridge such a scientific gap, the author was encouraged to propose a numerical solution for examining free transverse vibration of elastically supported DWCNTs under a more general circumference.

3.2. A discussion on the considered boundary conditions

In the proposed model in the previous section, a wide range of boundary conditions can be imposed to the model via rotary and transverse springs which are attached to the ends of the innermost and outermost tubes. Four rotary springs are aimed to control the rotations of the nanotubes' ends whereas their transverse motion can be controlled by transversely attached springs. These springs provide displacement boundary conditions, but what about the forced boundary conditions (for example, nonlocal resultant shear forces as well as nonlocal bending moments at the ends of the tubes) which are commonly expressed in terms of higher-order derivatives of transverse displacements? Herein it should be noticed that we are interested to study the problem via an efficient meshless methodology in which works with the weak form of Eqs. (6a) and (6b). As it will be seen, such conditions can be weakly (not strongly) satisfied by choosing appropriate values for constants of the attached springs to the nanotubes' ends.

On the other hand, as explained earlier, we are exploiting a simple version of the nonlocal continuum theory of Eringen, namely:

$$\sigma_{xx}^{nl} - (e_0 a)^2 \sigma_{xx,xx}^{nl} = \sigma_{xx}^{l} = E_b \, \epsilon_{xx} \tag{8}$$

for beam-like structures modeled by the NRBT, where σ_{xx}^{nl}, σ_{xx}^{l}, and ϵ_{xx} denote nonlocal longitudinal stress, local longitudinal stress, and longitudinal strain, respectively. In this research work, the nonlocal governing equations are simply constructed based on their classical version. Such a procedure have been extensively applied for nonlocal continuum-based modeling of nanostructures [41,35–37,54–60]. In contrast to such models, there are so-called nonlocal non-classical models in which explain that Eq. (8) cannot be directly applied to the classical governing equations [61–64]. In other words, for nonlocal stress analysis of solid nanostructures, the nonlocal stresses should be firstly evaluated in terms of strains using the nonlocal constitutive relations, for example Eq. (8) for beam-like nanostructures. Thereafter, such a nonlocal version of stresses can be employed in evaluating the total strain energy of the nanostructure (i.e., the histories of all strains are taken into account). Thereby, the resulting nonlocal stress and bending moment of the beam-like nanostructure would be expressed in terms of higher-order strains. As a result, the forced boundary conditions in their strong form are stated as a function of higher-order derivatives of transverse displacements. Application of the meshless to such novel nonlocal models for investigating vibrations of DWCNTs or even MWCNTs can be considered as a hot topic for future works.

4. Application of RKPM to the problem under study

In this section, a brief introduction to the one-dimensional RKPM is given at first. The calculations of RKPM shape functions and their derivatives up to the third-order are explained in some detail. Thereafter, RKPM is employed for spatial discretization of the unknown fields of the problem at hand.

4.1. An introduction to one-dimensional RKPM

Based on the works of Liu and his coworkers [45,46,65,66], a continuous approximation of an arbitrarily one-dimensional field $u(x)$, could be expressed by:

$$u^a(x) = \int_\Omega \phi_a^*(x; x-s)\, u(s)\, ds, \tag{9}$$

where Ω denotes the spatial domain of our interest, and the modified kernel function $\phi_a^*(x; x-s)$ is defined as:

$$\phi_a^*(x; x-s) = \phi_a(x-s)\, c(x; x-s); \;\; \phi_a(x-s) = \frac{1}{a}\,\phi\left(\frac{x-s}{a}\right), \tag{10}$$

where $c(x; x-s)$ is the correction function, $\phi_a(x-s)$ is the kernel or window function which is characterized by the choice of both the dilation parameter, a, and the function ϕ. The dilation parameter controls the support or influence domain of the kernel function. The main privilege of the RKPM with respect to the traditional smooth particle hydrodynamics (SPH) method is the incorporation of the correction function into its formulations. The main task of the newly introduced function is to reduce the difficulties raised from finite domain effect. Thereby, it is anticipated to reduce the generated errors throughout the computational domain, particularly in those regions close to the boundaries. The correction function is commonly stated in the following form:

$$c(x; x-s) = \sum_{i=0}^{N} b_i(x)(x-s)^i = \mathbf{H}^T(x-s)\mathbf{b}(x), \tag{11}$$

where $\mathbf{H}^T$ is the base function, and $\mathbf{b}$ contains the unknown coefficients:

$$\begin{aligned} &\mathbf{H}^T = [1, x, x^2, \ldots, x^N], \\ &\mathbf{b}^T(x) = [b_0(x), b_1(x), \ldots, b_N(x)], \end{aligned} \tag{12}$$

in view of Eq. (10), by substituting Eq. (11) into Eq. (9), one can obtain:

$$u^a(x) = \sum_{k=0}^{N}\sum_{n=0}^{\infty} \frac{(-1)^n}{n!}\, b_k(x)\, m_{n+k}(x)\, u^{(n)}(x), \tag{13}$$

where $u^{(0)}(x) = u(x), u^{(n)} = \frac{\partial^n u}{\partial x^n}; n > 1$, and $m_n(x)$ represents the moment function of order n, which is defined by:

$$m_n(x) = \int_\Omega (x-s)^n\, \phi_a(x-s)\, ds. \tag{14}$$

In order to satisfy the Nth order completeness condition for $u^a(x)$:

$$\sum_{k=0}^{N} b_k(x) m_k(x) = 1, \sum_{k=0}^{N} b_k(x) m_{n+k}(x) = 0; \quad n \geqslant 1, \tag{15}$$

by solving the set of linear equations in Eq. (15), the unknown parameters $b_k(x)$ are determined as:

$$\mathbf{b}(x) = \mathbf{M}^{-1}(x)\mathbf{H}(0), \tag{16}$$

where the moment matrix, $\mathbf{M}$, is defined as:

$$\mathbf{M}(x) = \begin{pmatrix} m_0(x) & m_1(x) & \dots & m_N(x) \\ m_1(x) & m_2(x) & \dots & m_{N+1}(x) \\ \vdots & \vdots & \ddots & \vdots \\ m_N(x) & M_{N+1}(x) & \dots & m_{2N}(x) \end{pmatrix}, \tag{17}$$

by substituting Eq. (16) into Eq. (11), and introducing Eqs. (10) and (11) to Eq. (9), the modified kernel function is obtained as:

$$\phi_a^*(x; x-s) = \mathbf{H}^T(x-s)\,\mathbf{M}^{-1}(x)\,\mathbf{H}(0)\,\phi_a(x-s). \tag{18}$$

As it is seen in Eq. (9), the approximate function has been expressed continuously in terms of modified function. For the sake of numerical analysis, the discretized version of the approximate function is commonly required. Using trapezoidal rule, $u^a(x)$ is now rewritten as:

$$u^a(x) = \sum_{I=1}^{NP} \phi_I(x)\, u_I, \tag{19}$$

where NP is the total number of RKPM's particles, u_I is the nodal parameter value of the Ith RKPM's particle, and $\phi_I(x)$ is its shape function which is expressed by:

$$\phi_I(x) = \phi^*(x; x - x_I)\triangle x_I, \tag{20}$$

where $\triangle x_I$ is the length of the one-dimensional domain associated with the Ith particle. For example, in the case of N uniformly distributed particles of RKPM for a domain of length l_b, $\triangle x_1 = \triangle x_N = \frac{l_b}{2(N-1)}$, and $\triangle x_i = \frac{l_b}{N-1}; 2 \leqslant i \leqslant N-1$. The first, the second, and the third derivatives of the RKPM's shape functions are evaluated as:

$$\phi_{I,x}(x) = \begin{pmatrix} \mathbf{H}^T(x-s)\mathbf{M}^{-1}(x)\phi_{a,x}(x;x-x_I) + \\ \mathbf{H}^T_{,x}(x-s)\mathbf{M}^{-1}(x)\phi_a(x;x-x_I) + \\ \mathbf{H}^T(x-s)\mathbf{M}^{-1}_{,x}(x)\phi_a(x;x-x_I) \end{pmatrix} \mathbf{H}(0)\,\triangle x_I, \tag{21a}$$

$$\phi_{I,xx}(x) = \begin{pmatrix} \mathbf{H}^T(x-s)\mathbf{M}^{-1}(x)\phi_{a,xx}(x;x-x_I) + \mathbf{H}^T_{,xx}(x-s)\mathbf{M}^{-1}(x)\phi_a(x;x-x_I) + \\ \mathbf{H}^T(x-s)\mathbf{M}^{-1}_{,xx}(x)\phi_a(x;x-x_I) + 2\mathbf{H}^T_{,x}(x-s)\mathbf{M}^{-1}(x)\phi_{a,x}(x;x-x_I) + \\ 2\mathbf{H}^T_{,x}(x-s)\mathbf{M}^{-1}_{,x}(x)\phi_a(x;x-x_I) + 2\mathbf{H}^T(x-s)\mathbf{M}^{-1}_{,x}(x)\phi_{a,x}(x;x-x_I) \end{pmatrix} \mathbf{H}(0)\triangle x_I, \tag{21b}$$

$$\phi_{I,xxx}(x) = \begin{pmatrix} \mathbf{H}^T(x-s)\mathbf{M}^{-1}(x)\phi_{a,xxx}(x;x-x_I) + \mathbf{H}^T_{,xxx}(x-s)\mathbf{M}^{-1}(x)\phi_a(x;x-x_I) + \\ \mathbf{H}^T(x-s)\mathbf{M}^{-1}_{,xxx}(x)\phi_a(x;x-x_I) + 3\mathbf{H}^T_{,x}(x-s)\mathbf{M}^{-1}(x)\phi_{a,xx}(x;x-x_I) + \\ 3\mathbf{H}^T(x-s)\mathbf{M}^{-1}_{,x}(x)\phi_{a,xx}(x;x-x_I) + 3\mathbf{H}^T_{,xx}(x-s)\mathbf{M}^{-1}(x)\phi_{a,x}(x;x-x_I) + \\ 3\mathbf{H}^T_{,xx}(x-s)\mathbf{M}^{-1}_{,x}(x)\phi_a(x;x-x_I) + 3\mathbf{H}^T(x-s)\mathbf{M}^{-1}_{,x}(x)\phi_{a,x}(x;x-x_I) + \\ 3\mathbf{H}^T_{,x}(x-s)\mathbf{M}^{-1}_{,xx}(x)\phi_a(x;x-x_I) + 6\mathbf{H}^T_{,x}(x-s)\mathbf{M}^{-1}_{,x}(x)\phi_{a,x}(x;x-x_I) \end{pmatrix} \mathbf{H}(0)\triangle x_I. \tag{21c}$$

Using the relation $\mathbf{M}(x)\,\mathbf{M}^{-1}(x) = \mathbf{I}$, where $\mathbf{I}$ is the identity matrix, $\mathbf{M}^{-1}_{,x}(x)$ and $\mathbf{M}^{-1}_{,xx}(x)$ are calculated as follows:

$$\begin{aligned}\mathbf{M}_{,x}^{-1} &= -\mathbf{M}^{-1}\mathbf{M}_{,x}\mathbf{M}^{-1},\\ \mathbf{M}_{,xx}^{-1} &= -\mathbf{M}^{-1}\mathbf{M}_{,xx}\mathbf{M}^{-1} + 2\mathbf{M}^{-1}\mathbf{M}_{,x}\mathbf{M}^{-1}\mathbf{M}_{,x}\mathbf{M}^{-1},\end{aligned} \tag{22}$$

by using the discretized form of Eq. (14), the first, second, and third derivatives of the elements of the moment matrix could be readily calculated as:

$$m_n(x) = \sum_{i=1}^{NP}(x-x_i)^n\phi_a(x-x_i)\,\triangle x_i, \tag{23a}$$

$$m_{n,x}(x) = \begin{cases}\sum_{i=1}^{NP}\phi_{a,x}(x-x_i)\,\triangle x_i; & n=0\\ \sum_{i=1}^{NP}(x-x_i)^{n-1}\big((x-x_i)\phi_{a,x}(x-x_i)+n\phi_a(x-x_i)\big)\,\triangle x_i; & n\geqslant 1\end{cases}, \tag{23b}$$

$$m_{n,xx}(x) = \begin{cases}\sum_{i=1}^{NP}\phi_{a,xx}(x-x_i)\,\triangle x_i; & n=0\\ \sum_{i=1}^{NP}\big((x-x_i)\phi_{a,xx}(x;x-x_i)+2\phi_{a,x}(x;x-x_i)\big)\,\triangle x_i; & n=1\\ \sum_{i=1}^{NP}\Big((x-x_i)^n\phi_{a,xx}(x;x-x_i)+2n(x-x_i)^{n-1}\phi_{a,x}(x;x-x_i)+n(n-1)(x-x_i)^{n-2}\phi_a(x-x_i)\Big)\,\triangle x_i; & n\geqslant 2\end{cases}, \tag{23c}$$

$$m_{n,xxx}(x) = \begin{cases}\sum_{i=1}^{NP}\phi_{a,xxx}(x-x_i)\,\triangle x_i; & n=0\\ \sum_{i=1}^{NP}\big((x-x_i)\phi_{a,xxx}(x;x-x_i)+3\phi_{a,xx}(x;x-x_i)\big)\,\triangle x_i; & n=1\\ \sum_{i=1}^{NP}\Big((x-x_i)^2\phi_{a,xxx}(x;x-x_i)+n(n+1)\phi_{a,x}(x;x-x_i)+2(n+1)(x-x_i)\phi_{a,xx}(x;x-x_i)\Big)\,\triangle x_i; & n=2\\ \sum_{i=1}^{NP}\Big((x-x_i)^n\phi_{a,xxx}(x;x-x_i)+3n(x-x_i)^{n-1}\phi_{a,xx}(x;x-x_i)+3n(n-1)(x-x_i)^{n-2}\phi_{a,x}(x;x-x_i)\\ \quad+n(n-1)(n-2)(x-x_i)^{n-3}\phi_a(x-x_i)\Big)\,\triangle x_i; & n\geqslant 3\end{cases}. \tag{23d}$$

In this article, linear base function (i.e., $\mathbf{H}^T(x)=[1,x]$), and the following function is employed for construction of the window and shape functions of RKPM:

$$\phi(x) = \exp\left(-\left(\frac{x}{\alpha}\right)^2\right);\quad \alpha = 0.3, \tag{24}$$

with $a=3.2$. In the case of using 7 RKPM's particles which are distributed uniformly over the spatial domain $[0,1]$, the plots of RKPM's shape functions as well as their first, second, and third derivatives are demonstrated in Fig. 2(a)–(d).

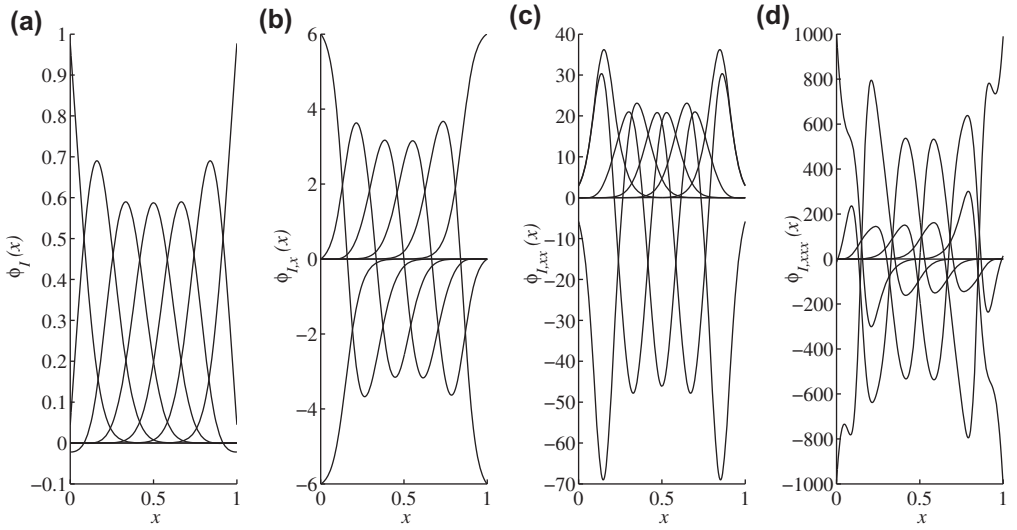

Fig. 2. The plots of: (a) RKPM's shape functions, (b) first derivative of RKPM's shape functions, (c) second derivative of RKPM's shape functions, (d) third derivative of RKPM's shape functions.

4.2. Solving the governing equations of DWCNTs using RKPM

For the numerical solving of the dimensionless equations of motion of elastically supported DWCNTs, both sides of Eqs. (6a) and (6b) are, respectively, multiplied by $\delta\overline{w}_1$ and $\delta\overline{w}_2$ where δ represents the variational sign. The sum of the resulting equations is then integrated over the normalized length of the DWCNT. After taking successful integration by parts, one can arrive at:

$$\begin{aligned}
&\int_0^1 \Big\{ \left(\delta\overline{w}_1 - \mu^2\delta\overline{w}_{1,\xi\xi}\right)\overline{w}_{1,\tau\tau} + \lambda_1^{-2}\left(\delta\overline{w}_{1,\xi}\overline{w}_{1,\xi\tau\tau} + \mu^2\delta\overline{w}_{1,\xi\xi}\overline{w}_{1,\xi\xi\tau\tau}\right) + \overline{C}_v\left(\delta\overline{w}_1 - \mu^2\delta\overline{w}_{1,\xi\xi}\right)\left(\overline{w}_1 - \overline{w}_2\right) + \delta\overline{w}_{1,\xi\xi}\overline{w}_{1,\xi\xi} \\
&+\overline{N}_{b_1}\left(\delta\overline{w}_{1,\xi}\overline{w}_{1,\xi} + \mu^2\delta\overline{w}_{1,\xi\xi}\overline{w}_{1,\xi\xi}\right) + \sum_{k=1}^{2}\left(\overline{K}_{z_1}(\xi_k)\left(\delta\overline{w}_1 - \mu^2\delta\overline{w}_{1,\xi\xi}\right)\overline{w}_1 + \overline{K}_{y_1}(\xi_k)\left(\delta\overline{w}_{1,\xi} - \mu^2\delta\overline{w}_{1,\xi\xi\xi}\right)\overline{w}_{1,\xi}\right)\delta(\xi-\xi_k) \\
&+\varrho_1^2\left(\delta\overline{w}_2 - \mu^2\delta\overline{w}_{2,\xi\xi}\right)\overline{w}_{2,\tau\tau} + \lambda_1^{-2}\varrho_2^2\left(\delta\overline{w}_{2,\xi}\overline{w}_{2,\xi\tau\tau} + \mu^2\delta\overline{w}_{2,\xi\xi}\overline{w}_{2,\xi\xi\tau\tau}\right) - \overline{C}_v\left(\delta\overline{w}_2 - \mu^2\delta\overline{w}_{2,\xi\xi}\right)\left(\overline{w}_1 - \overline{w}_2\right) + \varrho_3^2\delta\overline{w}_{2,\xi\xi}\overline{w}_{2,\xi\xi} \\
&+\overline{N}_{b_2}\left(\delta\overline{w}_{2,\xi}\overline{w}_{2,\xi} + \mu^2\delta\overline{w}_{2,\xi\xi}\overline{w}_{2,\xi\xi}\right) + \sum_{k=1}^{2}\left(\overline{K}_{z_2}(\xi_k)\left(\delta\overline{w}_2 - \mu^2\delta\overline{w}_{2,\xi\xi}\right)\overline{w}_2 + \overline{K}_{y_2}(\xi_k)\left(\delta\overline{w}_{2,\xi} - \mu^2\delta\overline{w}_{2,\xi\xi\xi}\right)\overline{w}_{2,\xi}\right)\delta(\xi-\xi_k) \\
&+\overline{K}_t\left(\delta\overline{w}_2 - \mu^2\delta\overline{w}_{2,\xi\xi}\right)\overline{w}_2 + \overline{K}_r\left(\delta\overline{w}_{2,\xi}\overline{w}_{2,\xi} + \mu^2\delta\overline{w}_{2,\xi\xi}\overline{w}_{2,\xi\xi}\right)\Big\}\,d\xi = 0.
\end{aligned} \tag{25}$$

The unknown fields associated with the elastically supported DWCNT embedded in an elastic medium are discretized in the spatial domain as: $\overline{w}_1(\xi,\tau) = \sum_{I=1}^{NP_1}\phi_I^{w_1}(\xi)\overline{w}_{1_I}(\tau)$ and $\overline{w}_2(\xi,\tau) = \sum_{I=1}^{NP_2}\phi_I^{w_2}(\xi)\overline{w}_{2_I}(\tau)$ where NP_1/NP_2, $\phi_I^{w_1}(\xi)/\phi_I^{w_2}(\xi)$, and $\overline{w}_{1_I}(\tau)/\overline{w}_{2_I}(\tau)$ denote the number of RKPMs particles, the RKPM shape functions pertinent to the Ith particle, and the nodal parameter values of the Ith particle of the innermost/outermost tubes, respectively. Therefore, Eq. (25) can be rewritten in the matrix form as follows:

$$\begin{bmatrix} [\overline{\mathbf{M}}_b]^{w_1w_1} & [\overline{\mathbf{M}}_b]^{w_1w_2} \\ [\overline{\mathbf{M}}_b]^{w_2w_1} & [\overline{\mathbf{M}}_b]^{w_2w_2} \end{bmatrix} \begin{Bmatrix} \overline{\mathbf{w}}_{1,\tau\tau} \\ \overline{\mathbf{w}}_{2,\tau\tau} \end{Bmatrix} + \begin{bmatrix} [\overline{\mathbf{K}}_b]^{w_1w_1} & [\overline{\mathbf{K}}_b]^{w_1w_2} \\ [\overline{\mathbf{K}}_b]^{w_2w_1} & [\overline{\mathbf{K}}_b]^{w_2w_2} \end{bmatrix} \begin{Bmatrix} \overline{\mathbf{w}}_1 \\ \overline{\mathbf{w}}_2 \end{Bmatrix} = \begin{Bmatrix} \mathbf{0} \\ \mathbf{0} \end{Bmatrix}, \tag{26}$$

where the nonzero submatrices in Eq. (26) are as:

$$[\overline{\mathbf{M}}_b]_{IJ}^{w_1w_1} = \int_0^1 \left(\phi_I^{w_1}\phi_J^{w_1} + \lambda^{-2}\phi_{I,\xi}^{w_1}\phi_{J,\xi}^{w_1} - \mu^2\phi_{I,\xi\xi}^{w_1}\left(\phi_J^{w_1} - \lambda^{-2}\phi_{J,\xi\xi}^{w_1}\right)\right)\mathrm{d}\xi, \tag{27a}$$

$$[\overline{\mathbf{M}}_b]_{IJ}^{w_2w_2} = \int_0^1 \left(\varrho_1^2\phi_I^{w_2}\phi_J^{w_2} + \varrho_2^2\lambda^{-2}\phi_{I,\xi}^{w_2}\phi_{J,\xi}^{w_2} - \mu^2\phi_{I,\xi\xi}^{w_2}\left(\varrho_1^2\phi_J^{w_2} - \lambda^{-2}\varrho_2^2\phi_{J,\xi\xi}^{w_2}\right)\right)\mathrm{d}\xi, \tag{27b}$$

$$\begin{aligned}
[\overline{\mathbf{K}}_b]_{IJ}^{w_1w_1} = &\int_0^1 \left(\phi_{I,\xi\xi}^{w_1}\phi_{J,\xi\xi}^{w_1} + \overline{N}_{b_1}\left(\phi_{I,\xi}^{w_1}\phi_{J,\xi}^{w_1} + \mu^2\phi_{I,\xi\xi}^{w_1}\phi_{J,\xi\xi}^{w_1}\right) + \overline{C}_v\left(\phi_I^{w_1} - \mu^2\phi_{I,\xi\xi}^{w_1}\right)\phi_J^{w_1}\right)\mathrm{d}\xi \\
&+\sum_{k=1}^{2}\left(\overline{K}_{z_1}(\xi_k)\left(\phi_I^{w_1}(\xi_k) - \mu^2\phi_{I,\xi\xi}^{w_1}(\xi_k)\right)\phi_J^{w_1}(\xi_k) + \overline{K}_{y_1}(\xi_k)\left(\phi_{I,\xi}^{w_1}(\xi_k) - \mu^2\phi_{I,\xi\xi\xi}^{w_1}(\xi_k)\right)\phi_{J,\xi}^{w_1}(\xi_k)\right),
\end{aligned} \tag{27c}$$

$$[\overline{\mathbf{K}}_b]_{IJ}^{w_1w_2} = -\int_0^1 \overline{C}_v\left(\phi_I^{w_1} - \mu^2\phi_{I,\xi\xi}^{w_1}\right)\phi_J^{w_2}\mathrm{d}\xi, \tag{27d}$$

$$[\overline{\mathbf{K}}_b]_{IJ}^{w_2w_1} = -\int_0^1 \overline{C}_v\left(\phi_I^{w_2} - \mu^2\phi_{I,\xi\xi}^{w_2}\right)\phi_J^{w_1}\mathrm{d}\xi, \tag{27e}$$

$$\begin{aligned}
[\overline{\mathbf{K}}_b]_{IJ}^{w_2w_2} = &\int_0^1 \begin{pmatrix} \varrho_3^2\phi_{I,\xi\xi}^{w_2}\phi_{J,\xi\xi}^{w_2} + \overline{N}_{b_2}\left(\phi_{I,\xi}^{w_2}\phi_{J,\xi}^{w_2} + \mu^2\phi_{I,\xi\xi}^{w_2}\phi_{J,\xi\xi}^{w_2}\right) + \overline{C}_v\left(\phi_I^{w_2} - \mu^2\phi_{I,\xi\xi}^{w_2}\right)\phi_J^{w_2} \\ +\overline{K}_t\left(\phi_I^{w_2} - \mu^2\phi_{I,\xi\xi}^{w_2}\right)\phi_J^{w_2} + \overline{K}_r\left(\phi_{I,\xi}^{w_2} - \mu^2\phi_{I,\xi\xi\xi}^{w_2}\right)\phi_J^{w_2} \end{pmatrix}\mathrm{d}\xi \\
&+\sum_{k=1}^{2}\left(\overline{K}_{z_2}(\xi_k)\left(\phi_I^{w_2}(\xi_k) - \mu^2\phi_{I,\xi\xi}^{w_2}(\xi_k)\right)\phi_J^{w_2}(\xi_k) + \overline{K}_{y_2}(\xi_k)\left(\phi_{I,\xi}^{w_2}(\xi_k) - \mu^2\phi_{I,\xi\xi\xi}^{w_2}(\xi_k)\right)\phi_{J,\xi}^{w_2}(\xi_k)\right).
\end{aligned} \tag{27f}$$

For calculating the natural flexural frequencies of the DWCNT, one can assume: $\overline{\mathbf{w}}_1(\tau) = \overline{\mathbf{w}}_{1_0}e^{\mathrm{i}\varpi\tau}$ and $\overline{\mathbf{w}}_2(\tau) = \overline{\mathbf{w}}_{2_0}e^{\mathrm{i}\varpi\tau}$ where $\mathrm{i} = \sqrt{-1}$, $\overline{\mathbf{w}}_{1_0}$ and $\overline{\mathbf{w}}_{2_0}$ are the initial nodal parameter vectors of the innermost and outermost tubes, respectively, and ϖ denotes the dimensionless flexural frequency of the DWCNT embedded in an elastic matrix under initially axial force. By substituting these new forms of $\overline{\mathbf{w}}_1$ and $\overline{\mathbf{w}}_2$ into Eq. (26),

$$\left(-\varpi^2\begin{bmatrix} [\overline{\mathbf{M}}_b]^{w_1w_1} & [\overline{\mathbf{M}}_b]^{w_1w_2} \\ [\overline{\mathbf{M}}_b]^{w_2w_1} & [\overline{\mathbf{M}}_b]^{w_2w_2} \end{bmatrix} + \begin{bmatrix} [\overline{\mathbf{K}}_b]^{w_1w_1} & [\overline{\mathbf{K}}_b]^{w_1w_2} \\ [\overline{\mathbf{K}}_b]^{w_2w_1} & [\overline{\mathbf{K}}_b]^{w_2w_2} \end{bmatrix}\right)\begin{Bmatrix} \overline{\mathbf{w}}_{1_0} \\ \overline{\mathbf{w}}_{2_0} \end{Bmatrix} = \begin{Bmatrix} \mathbf{0} \\ \mathbf{0} \end{Bmatrix}. \tag{28}$$

Through solving the set of eigenvalue equations in Eq. (28), the eigenvalues (i.e., dimensionless flexural frequencies) and the corresponding eigenvectors (i.e., flexural vibration modes) of a lengthy DWCNT embedded in an elastic matrix under initially axial force are obtained based on the NRBT hypotheses.

5. Results and discussion

In this section, the capability of the proposed numerical model in capturing the natural frequencies of DWCNTs is initially explored through some comparisons of the obtained results with those of other works. Subsequently, the first five natural frequencies of DWCNTs for different boundary conditions, slenderness ratios, small-scale parameters, and initially axial forces will be presented in the tabular format. Afterward, the effects of various factors on the first five dimensionless flexural frequencies of DWCNTs with different boundary conditions will be presented graphically. For this purpose, consider a DWCNT of length 20 nm, consisting of the innermost and outermost tubes of mean radii 0.5 nm and 0.84 nm, respectively, whose walls' thickness is equal to 0.34 nm. The material properties of the innermost and outermost tubes of the DWCNT are as: $\rho_{b_i} = 2500\ \mathrm{kg/m^3}$ and E_{b_i}=1 TPa. Throughout this section, the above-mentioned values are used in the frequency analysis of the problem unless other values are clearly specified for the aforementioned parameters. The nth dimensionless frequency associated with the nth vibration mode of the DWCNT is now defined by $\Omega_n = \sqrt{\varpi_n}$. In the RKPM analysis of each tube, 11 uniformly distributed particles, cubic spline window function, and linear base function are used. The dilation parameter pertinent to each particle is set equal to 3.2. Additionally, similar RKPM shape functions are employed for discretization of the deflection fields of the innermost and outermost tubes. For different boundary conditions, the values of the parameters $\overline{K}_{y_i}$ and $\overline{K}_{z_i}$ have been given in Table 1. In Table 1, SS and CC stand for fully simply supported and fully clamped conditions of both the innermost and outermost tubes, respectively. The S_fS or S_fC conditions imply that the left ends of both tubes are shear-free whereas their right ends have simply supported or clamped supports. The condition SC denotes that the left ends of both tubes have simple supports while the right ends have clamped supports. Finally, the CF condition implies that the left supports of both tubes are clamped whereas the right ones are free from any constraint (i.e., cantilevered DWCNT).

5.1. Comparison of the obtained results with those of other works

In order to check the accuracy of the numerical calculations, the predicted results by the proposed model are verified with those of other available works in some particular cases. In the first verification, the obtained results are compared with those of Aydogdu [21]. In the carried out work by Aydogdu [21], the parameter C_v was approximated by $C_v = 320 \times (2r_{m_1})/0.16d^2\ (\mathrm{erg/cm^2})$ where d = 0.142 nm. Furthermore, for the sake of comparability of the obtained results with those of Aydogdu [21], the nth nondimensional natural frequency of the DWCNT is now introduced by $\Xi_n = (\frac{\rho_{b_1} A_b l_b^4}{E_{b_1} I_b} \omega_n^2)^{\frac{1}{4}}$ where $\omega_n = \sqrt{E_{b_1} I_{b_1}/(\rho_{b_1} A_{b_1} l_b^4)}\,\varpi_n, A_b = A_{b_1} + A_{b_2}$, and $I_b = I_{b_1} + I_{b_2}$. In the work of Aydogdu [21], the natural frequencies of multi-walled carbon nanotubes were obtained in the case of simply supported conditions using a higher-order beam theory. The predicted first five nondimensional flexural frequencies by Aydogdu [21] as well as those of the proposed model have been provided in Table 2. The results are given for two levels of the aspect ratio of the DWCNT, l_b/r_{m_1} = 20 and 100. As it is seen in Table 2, the proposed numerical model can reproduce the nondimensional flexural frequencies of the DWCNT by Aydogdu [21] with a good accuracy.

Table 1
The values of $\overline{K}_{y_i}$ and $\overline{K}_{z_i}$ for the considered boundary conditions.

	SS	CC	SC	S_fS	S_fC	CF
$\overline{K}_{z_i}(\xi_1)$	10^8	10^8	10^8	0	0	10^8
$\overline{K}_{z_i}(\xi_2)$	10^8	10^8	10^8	10^8	10^8	0
$\overline{K}_{y_i}(\xi_1)$	0	10^8	0	10^8	10^8	10^8
$\overline{K}_{y_i}(\xi_2)$	0	10^8	10^8	0	10^8	0

Table 2
Comparison between the predicted first five nondimensional frequencies of the DWCNT via RKPM and those of Aydogdu [21].

l_b/r_{m_2}		Ξ_1	Ξ_2	Ξ_3	Ξ_4	Ξ_5
20	Aydogdu [21]	3.1410	6.2650	9.2756	11.880	13.946
	Proposed model	3.1331	6.2080	9.1118	11.6232	12.7541
100	Aydogdu [21]	3.1416	6.2832	9.4245	12.565	15.705
	Proposed model	3.1411	6.2835	9.4286	12.5810	15.7503

In another comparison study, without taking into account the nonlocal effect, the predicted first and second flexural frequencies of the DWCNT are compared with those of the proposed analytical model by Wang and Varadan [37]. The analytical expressions of the natural frequencies of DWCNTs by Wang and Varadan [37] were limited to DWCNTs with simply supported conditions. The considered geometry, physical, and mechanical data of the DWCNTs are identical to those mentioned in Ref. [37]. To cover a wide range of the aspect ratio and to assess the effect of the aspect ratio on the vibration characteristics of the DWCNT, five levels of the length for the DWCNT and three levels of the radius of the innermost tube have been taken into account (see Table 3). As it is clear from Table 3, there is a good agreement between the obtained frequencies by the proposed model and those of Wang and Varadan [37]. Moreover, both the first and second natural frequencies of the DWCNT increase with the radius of the innermost tube whereas decrease with the length of the DWCNT.

In another comparison, the dimensionless fundamental frequency of the DWCNT based on the proposed model are verified with those of the model proposed by Ke et al. [67]. Using nonlocal Timoshenko beam theory, Ke et al. [67] studied vibrations of DWCNTs using differential quadrature method (DQM). The DWCNT under study has the following properties: $\rho_{b_i} = 2300\ \text{kg/m}^3$, $E_{b_i} = 1$ TPa, $r_{m_1} = 0.35$ nm, $r_{m_2} = 0.7$ nm, $t_{b_i} = 0.35$ nm, $l_b = 20 r_{m_2}$, and $K_t = K_r = N_{b_i} = 0; i = 1, 2$. In Table 4, the predicted results by the proposed numerical model and those of Ke et al. [67] are provided for SS, CC, and SC boundary conditions and four levels of the small-scale parameter. As it is seen in Table 4, for all levels of the small-scale parameter, the present model can capture the results of Ke et al. [67] for SS, CC, and SC boundary conditions with relative error lower than 2.2, 6.5, and 5.8 percent, respectively. By increasing the small-scale parameter, the discrepancies between the results of two models would decrease. Furthermore, the predicted results by the proposed model are generally greater than those of the model by Ke et al. [67]. It is mainly related to this fact that the Rayleigh beam model does not consider the shear deformation effects of the nanostructure. In other words, its transverse stiffness is commonly overestimated with respect to the Timoshenko beam model. As a result, the resulting frequencies of the nanostructure are generally higher than those obtained by Timoshenko beam theory. Additionally, such discrepancies is expected to become highlighted as the nanostructure's length decreases.

5.2. Numerical study of the effects of small-scale parameter and initially applied force on the first five natural frequencies of DWCNTs for different boundary conditions as well as slenderness ratio

For the proposed model, the first five dimensionless frequencies of DWCNTs with SS, CC, SC, S_fS, S_fC, and CF boundary conditions are provided in Tables 5–10, respectively. The results have been given for four levels of the slenderness ratio of the innermost tube (i.e., $\lambda_1 = 40, 60, 80,$ and 120) as well as four levels of the small-scale parameter

Table 3
Comparison of the predicted first two natural frequencies of the DWCNT by the proposed model with those of Wang and Varadan [37] for DWCNTs with various levels of length and radius of the innermost tube.

$l_b$nm	ω_1 (THz)						ω_2 (THz)					
	r_{m_1} = 0.5 nm		r_{m_1} = 0.75 nm		r_{m_1} = 1 nm		r_{m_1} = 0.5 nm		r_{m_1} = 0.75 nm		r_{m_1} = 1 nm	
	WV[a]	PS[b]	WV	PS	WV	PS	WV	PS	WV	PS	WV	PS
14	0.7416	0.7419	0.9783	0.9684	1.2214	1.2030	2.8321	2.9687	3.7072	3.8738	4.6180	4.8103
18	0.4494	0.4488	0.5931	0.5859	0.7406	0.7278	1.7694	1.7966	2.3268	2.3450	2.8996	2.9126
22	0.3010	0.3004	0.3973	0.3922	0.4962	0.4872	1.1958	1.2029	1.5758	1.5701	1.9960	1.9504
26	0.2156	0.2151	0.2845	0.2808	0.3554	0.3488	0.8593	0.8612	1.1322	1.1243	1.4146	1.3966
30	0.1619	0.1616	0.2137	0.2109	0.2669	0.2620	0.6465	0.6469	0.8529	0.8445	1.0649	1.0490

[a] The expression WV stands for Wang and Varadan [37].
[b] The expression PS stands for present study.

Table 4
Comparison of the dimensionless fundamental frequency (i.e., $\overline{\omega}_1$) of the DWCNT based on the present work with those of Ke et al. [67] for SS, CC, and SC boundary conditions and various values of the small-scale parameter.

BCs[a]	Model (approach)	Dimensionless fundamental frequency: $\overline{\omega}_1$[b]		
		$\mu = 0.1$	$\mu = 0.15$	$\mu = 0.2$
SS	Ke et al. [67] (DQM)	0.2920	0.2768	0.2591
	Present work (RKPM)	0.2984	0.2830	0.2649
CC	Ke et al. [67] (DQM)	0.6055	0.5687	0.5266
	Present work (RKPM)	0.6449	0.5942	0.5396
SC	Ke et al. [67] (DQM)	0.4366	0.4112	0.3820
	Present work (RKPM)	0.4618	0.4316	0.3976

[a] boundary conditions.
[b] $\overline{\omega}_1 = \omega_1 l_b \sqrt{\rho_b / E_b}$.

Table 5
The first five dimensionless frequencies of a DWCNT with SS boundary conditions for various values of slenderness ratio, small-scale parameter, and initially axial force.

λ_1	$e_0a = 0$ nm			$e_0a = 1$ nm			$e_0a = 1.5$ nm			$e_0a = 2$ nm		
	$\overline{N}_{b_i} = 0$	$\overline{N}_{b_i} = 10$	$\overline{N}_{b_i} = 20$	$\overline{N}_{b_i} = 0$	$\overline{N}_{b_i} = 10$	$\overline{N}_{b_i} = 20$	$\overline{N}_{b_i} = 0$	$\overline{N}_{b_i} = 10$	$\overline{N}_{b_i} = 20$	$\overline{N}_{b_i} = 0$	$\overline{N}_{b_i} = 10$	$\overline{N}_{b_i} = 20$
40	3.7344	4.0433	4.2942	3.6946	4.0121	4.2683	3.6476	3.9758	4.2383	3.5866	3.9291	4.2000
	7.3937	7.5625	7.7207	7.1021	7.2915	7.4671	6.8057	7.0195	7.2153	6.4764	6.7221	6.9434
	10.8863	11.0040	11.1180	10.0326	10.1809	10.3228	9.3101	9.4933	9.6663	8.6183	8.8460	9.0571
	14.0984	14.1959	14.2911	12.4267	12.5617	12.6922	11.2344	11.4118	11.5809	10.2110	10.4417	10.6574
	16.9139	17.0073	17.0989	14.3221	14.4573	14.5882	12.7107	12.8927	13.0664	11.4228	11.6638	11.8896
60	3.7411	4.0503	4.3016	3.7231	4.0362	4.2898	3.7012	4.0191	4.2757	3.6715	3.9961	4.2567
	7.4501	7.6188	7.7769	7.3117	7.4898	7.6559	7.1553	7.3448	7.5206	6.9617	7.1666	7.3554
	11.0911	11.2058	11.3171	10.6536	10.7827	10.9073	10.2091	10.3553	10.4956	9.7151	9.8840	10.0447
	14.6221	14.7098	14.7959	13.6736	13.7802	13.8843	12.8199	12.9484	13.0732	11.9642	12.1213	12.2724
	17.9942	18.0671	18.1391	16.3369	16.4325	16.5264	15.0161	15.1376	15.2562	13.8024	13.9571	14.1068
80	3.7434	4.0528	4.3042	3.7332	4.0448	4.2975	3.7207	4.0350	4.2894	3.7034	4.0216	4.2783
	7.4691	7.6380	7.7963	7.3894	7.5636	7.7265	7.2955	7.4762	7.6447	7.1734	7.3632	7.5392
	11.1582	11.2727	11.3838	10.8991	11.0218	11.1406	10.6133	10.7461	10.8741	10.2687	10.4150	10.5553
	14.7893	14.8759	14.9610	14.2059	14.3034	14.3990	13.6131	13.7238	13.8318	12.9544	13.0825	13.2069
	18.3384	18.4084	18.4776	17.2703	17.3539	17.4362	16.2789	16.3783	16.4759	15.2605	15.3807	15.4982
120	3.7450	4.0546	4.3061	3.7405	4.0510	4.3031	3.7348	4.0466	4.2994	3.7270	4.0404	4.2943
	7.4824	7.6515	7.8100	7.4464	7.6178	7.7784	7.4026	7.5770	7.7401	7.3433	7.5218	7.6884
	11.2043	11.3190	11.4302	11.0848	11.2031	11.3178	10.9439	11.0668	11.1858	10.7607	10.8899	11.0147
	14.9022	14.9886	15.0736	14.6253	14.7168	14.8065	14.3125	14.4100	14.5056	13.9251	14.0309	14.1344
	18.5669	18.6363	18.7049	18.0419	18.1174	18.1921	17.4777	17.5608	17.6427	16.8155	16.9087	17.0005

Table 6
The first five dimensionless frequencies of a DWCNT with CC boundary conditions for various values of slenderness ratio, small-scale parameter, and initially axial force.

λ_1	$e_0a = 0$ nm			$e_0a = 1$ nm			$e_0a = 1.5$ nm			$e_0a = 2$ nm		
	$\overline{N}_{b_i} = 0$	$\overline{N}_{b_i} = 10$	$\overline{N}_{b_i} = 20$	$\overline{N}_{b_i} = 0$	$\overline{N}_{b_i} = 10$	$\overline{N}_{b_i} = 20$	$\overline{N}_{b_i} = 0$	$\overline{N}_{b_i} = 10$	$\overline{N}_{b_i} = 20$	$\overline{N}_{b_i} = 0$	$\overline{N}_{b_i} = 10$	$\overline{N}_{b_i} = 20$
40	5.7337	5.8549	5.9686	5.6397	5.7804	5.9110	5.5243	5.6884	5.8390	5.3808	5.5760	5.7522
	9.3964	9.4987	9.5976	8.9041	9.0370	9.1641	8.4229	8.5908	8.7491	7.9168	8.1287	8.3251
	12.8516	12.9374	13.0213	11.6323	11.7573	11.8783	10.6615	10.8293	10.9894	9.7777	9.9984	10.2050
	15.9293	16.0111	16.0913	13.7840	13.9110	14.0342	12.3370	12.5119	12.6791	11.1374	11.3714	11.5909
	17.5779	17.5834	17.5888	15.4466	15.5824	15.7140	13.6084	13.7945	13.9720	12.1727	12.4215	12.6544
60	5.7484	5.8696	5.9832	5.7100	5.8399	5.9612	5.6555	5.7961	5.9268	5.5829	5.7383	5.8816
	9.4957	9.5966	9.6942	9.2661	9.3810	9.4917	9.0024	9.1342	9.2604	8.6865	8.8407	8.9871
	13.1793	13.2595	13.3381	12.5451	12.6439	12.7405	11.9148	12.0355	12.1526	11.2424	11.3913	11.5344
	16.7226	16.7900	16.8565	15.4534	15.5437	15.6325	14.3544	14.4707	14.5843	13.2952	13.4445	13.5889
	20.0661	20.1264	20.1861	17.9734	18.0601	18.1456	16.3778	16.4938	16.6073	14.9605	15.1133	15.2614
80	5.7533	5.8745	5.9882	5.7344	5.8604	5.9784	5.7034	5.8356	5.9589	5.6607	5.8014	5.9322
	9.5273	9.6281	9.7256	9.3993	9.5080	9.6129	9.2392	9.3577	9.4718	9.0348	9.1666	9.2928
	13.2804	13.3598	13.4379	12.9080	12.9983	13.0867	12.4942	12.5974	12.6981	12.0090	12.1293	12.2462
	16.9625	17.0280	17.0927	16.1787	16.2576	16.3353	15.3944	15.4891	15.5820	14.5502	14.6655	14.7781
	20.5462	20.6023	20.6580	19.1770	19.2490	19.3202	17.9413	18.0315	18.1204	16.7123	16.8260	16.9375
120	5.7566	5.8779	5.9916	5.7509	5.8742	5.9898	5.7378	5.8639	5.9819	5.7186	5.8485	5.9699
	9.5488	9.6496	9.7472	9.4952	9.5995	9.7004	9.4211	9.5299	9.6350	9.3203	9.4352	9.5460
	13.3475	13.4269	13.5049	13.1809	13.2652	13.3478	12.9750	13.0653	13.1537	12.7096	12.8080	12.9042
	17.1187	17.1837	17.2480	16.7512	16.8223	16.8926	16.3293	16.4079	16.4854	15.8151	15.9038	15.9910
	20.8532	20.9081	20.9627	20.1805	20.2428	20.3045	19.4586	19.5297	19.6000	18.6284	18.7113	18.7931

(i.e., e_0a = 0, 1, 1.5, and 2 nm). For each pair of the slenderness ratio and small-scale parameter, the results are also provided for three values of initially applied axial force on both the innermost and outermost tubes (i.e., $\overline{N}_{b_i}$ = 0, 10, and 20; i = 1,2). As it is seen in Tables 5–10, for a constant level of the slenderness ratio, the dimensionless flexural frequencies generally decrease with an increase of the small-scale effect parameter. This matter is more apparent for higher modes of vibration. For specified values of small-scale parameter and initially axial force, the dimensionless frequencies increase with the slenderness ratio of the nanotube, irrespective of the boundary conditions of the DWCNT. This fact is more obvious for higher modes of vibration. Furthermore, an increase of the initially applied axial forces leads to an increase of the dimensionless

Table 7
The first five dimensionless frequencies of a DWCNT with SC boundary conditions for various values of slenderness ratio, small-scale parameter, and initially axial force.

λ_1	$e_0a = 0$ nm			$e_0a = 1$ nm			$e_0a = 1.5$ nm			$e_0a = 2$ nm		
	$\overline{N}_{b_i} = 0$	$\overline{N}_{b_i} = 10$	$\overline{N}_{b_i} = 20$	$\overline{N}_{b_i} = 0$	$\overline{N}_{b_i} = 10$	$\overline{N}_{b_i} = 20$	$\overline{N}_{b_i} = 0$	$\overline{N}_{b_i} = 10$	$\overline{N}_{b_i} = 20$	$\overline{N}_{b_i} = 0$	$\overline{N}_{b_i} = 10$	$\overline{N}_{b_i} = 20$
40	4.7127	4.9066	5.0789	4.6486	4.8568	5.0404	4.5707	4.7963	4.9932	4.4714	4.7203	4.9344
	8.3881	8.5178	8.6418	8.0060	8.1613	8.3081	7.6247	7.8096	7.9821	7.2129	7.4360	7.6405
	11.8669	11.9665	12.0634	10.8409	10.9754	11.1049	9.9981	10.1715	10.3362	9.2113	9.4336	9.6410
	15.0204	15.1089	15.1956	13.1181	13.2479	13.3737	11.7996	11.9747	12.1419	10.6884	10.9198	11.1367
	17.5551	17.5624	17.5688	14.8979	15.0327	15.1632	13.1723	13.3557	13.5307	11.8093	12.0538	12.2828
60	4.7231	4.9171	5.0896	4.6957	4.8961	5.0737	4.6592	4.8675	5.0513	4.6100	4.8293	5.0215
	8.4632	8.5922	8.7155	8.2838	8.4244	8.5583	8.0786	8.2334	8.3798	7.8287	8.0025	8.1655
	12.1259	12.2212	12.3142	11.5971	11.7089	11.8176	11.0648	11.1961	11.3229	10.4851	10.6420	10.7921
	15.6651	15.7416	15.8169	14.5651	14.6625	14.7579	13.5932	13.7146	13.8328	12.6381	12.7903	12.9372
	19.0264	19.0924	19.1577	17.1601	17.2506	17.3397	15.7047	15.8229	15.9383	14.3902	14.5434	14.6918
80	4.7266	4.9207	5.0933	4.7123	4.9099	5.0853	4.6914	4.8936	5.0726	4.6627	4.8712	5.0551
	8.4879	8.6169	8.7403	8.3864	8.5220	8.6514	8.2625	8.4063	8.5430	8.1028	8.2578	8.4044
	12.2083	12.3032	12.3959	11.8968	12.0011	12.1028	11.5511	11.6669	11.7794	11.1398	11.2710	11.3978
	15.8653	15.9403	16.0142	15.1878	15.2750	15.3607	14.5038	14.6055	14.7050	13.7557	13.8764	13.9940
	19.4325	19.4950	19.5569	18.2216	18.2988	18.3750	17.1124	17.2066	17.2994	15.9912	16.1076	16.2216
120	4.7291	4.9232	5.0959	4.7238	4.9195	5.0934	4.7148	4.9125	5.0880	4.7018	4.9024	5.0801
	8.5050	8.6341	8.7577	8.4610	8.5931	8.7193	8.4035	8.5392	8.6688	8.3254	8.4662	8.6004
	12.2642	12.3591	12.4518	12.1228	12.2220	12.3188	11.9517	12.0561	12.1579	11.7300	11.8417	11.9503
	15.9982	16.0729	16.1466	15.6789	15.7591	15.8382	15.3146	15.4016	15.4872	14.8669	14.9631	15.0575
	19.6974	19.7590	19.8200	19.1026	19.1710	19.2387	18.4633	18.5399	18.6155	17.7204	17.8079	17.8941

Table 8
The first five dimensionless frequencies of a DWCNT with S_fS boundary conditions for various values of slenderness ratio, small-scale parameter, and initially axial force.

λ_1	$e_0a = 0$ nm			$e_0a = 1$ nm			$e_0a = 1.5$ nm			$e_0a = 2$ nm		
	$\overline{N}_{b_i} = 0$	$\overline{N}_{b_i} = 10$	$\overline{N}_{b_i} = 20$	$\overline{N}_{b_i} = 0$	$\overline{N}_{b_i} = 10$	$\overline{N}_{b_i} = 20$	$\overline{N}_{b_i} = 0$	$\overline{N}_{b_i} = 10$	$\overline{N}_{b_i} = 20$	$\overline{N}_{b_i} = 0$	$\overline{N}_{b_i} = 10$	$\overline{N}_{b_i} = 20$
40	1.8813	2.3574	2.6490	1.8768	2.3552	2.6475	1.8705	2.3521	2.6455	1.8618	2.3479	2.6426
	5.6076	5.8239	6.0184	5.4787	5.7098	5.9158	5.3343	5.5835	5.8031	5.1603	5.4336	5.6709
	9.2151	9.3509	9.4810	8.6784	8.8403	8.9936	8.1779	8.3701	8.5497	7.6645	7.8957	8.1081
	12.5993	12.7030	12.8039	11.3504	11.4888	11.6222	10.3824	10.5601	10.7290	9.5107	9.7381	9.9501
	15.6349	15.7281	15.8194	13.4902	13.6236	13.7527	12.0682	12.2468	12.4172	10.8968	11.1321	11.3526
60	1.8821	2.3584	2.6501	1.8804	2.3576	2.6496	1.8776	2.3562	2.6487	1.8737	2.3543	2.6474
	5.6308	5.8474	6.0423	5.5724	5.7955	5.9955	5.5013	5.7328	5.9392	5.4088	5.6516	5.8667
	9.3304	9.4650	9.5940	9.0682	9.2147	9.3546	8.7833	8.9443	9.0971	8.4490	8.6295	8.7993
	12.9414	13.0391	13.1347	12.2717	12.3862	12.4976	11.6273	11.7617	11.8916	10.9491	11.1095	11.2631
	16.4176	16.4958	16.5728	15.1271	15.2262	15.3235	14.0325	14.1559	14.2762	12.9860	13.1407	13.2900
80	1.8824	2.3588	2.6505	1.8817	2.3584	2.6503	1.8801	2.3577	2.6498	1.8779	2.3566	2.6491
	5.6388	5.8555	6.0506	5.6062	5.8266	6.0245	5.5647	5.7899	5.9915	5.5090	5.7407	5.9473
	9.3686	9.5032	9.6323	9.2169	9.3583	9.4935	9.0403	9.1901	9.3329	8.8187	8.9799	9.1329
	13.0517	13.1488	13.2438	12.6494	12.7562	12.8604	12.2192	12.3377	12.4528	11.7211	11.8553	11.9851
	16.6649	16.7411	16.8163	15.8549	15.9434	16.0305	15.0639	15.1672	15.2683	14.2203	14.3429	14.4624
120	1.8826	2.3590	2.6508	1.8825	2.3590	2.6508	1.8819	2.3587	2.6506	1.8809	2.3582	2.6503
	5.6443	5.8613	6.0565	5.6304	5.8489	6.0454	5.6117	5.8323	6.0304	5.5858	5.8093	6.0097
	9.3951	9.5299	9.6592	9.3271	9.4649	9.5969	9.2429	9.3845	9.5200	9.1307	9.2776	9.4178
	13.1267	13.2238	13.3189	12.9403	13.0418	13.1410	12.7215	12.8284	12.9327	12.4432	12.5575	12.6687
	16.8301	16.9060	16.9808	16.4412	16.5227	16.6030	16.0083	16.0967	16.1836	15.4859	15.5836	15.6795

frequencies of the DWCNT for different boundary conditions. In the case of a DWCNT with SS boundary conditions (see Table 5), the effect of variation of initially axial force on the variation of flexural frequencies of the DWCNT with higher small-scale parameter is more obvious. However, for a lengthy DWCNT (i.e., a DWCNT with higher values of the slenderness ratio), the variation of initially axial forces as a function of flexural frequencies is not generally sensitive to the small-scale parameter. Moreover, for specified values of slenderness ratio and initially axial forces, the dimensionless flexural frequencies decrease with the small-scale parameter. Concerning free flexural vibration of a DWCNT with CC boundary conditions and a low level of the slenderness ratio (i.e., $\lambda_1 = 40$) (see Table 6), the first dimensionless frequency decreases with the small-scale

Table 9
The first five dimensionless frequencies of a DWCNT with S_fC boundary conditions for various values of slenderness ratio, small-scale parameter, and initially axial force.

λ_1	$e_0a = 0$ nm			$e_0a = 1$ nm			$e_0a = 1.5$ nm			$e_0a = 2$ nm		
	$\overline{N}_{b_i} = 0$	$\overline{N}_{b_i} = 10$	$\overline{N}_{b_i} = 20$	$\overline{N}_{b_i} = 0$	$\overline{N}_{b_i} = 10$	$\overline{N}_{b_i} = 20$	$\overline{N}_{b_i} = 0$	$\overline{N}_{b_i} = 10$	$\overline{N}_{b_i} = 20$	$\overline{N}_{b_i} = 0$	$\overline{N}_{b_i} = 10$	$\overline{N}_{b_i} = 20$
40	2.8574	3.0778	3.2567	2.8475	3.0759	3.2603	2.8321	3.0707	3.2619	2.8111	3.0637	3.2640
	6.6031	6.7566	6.9000	6.4210	6.5945	6.7552	6.2179	6.4156	6.5964	5.9797	6.2089	6.4152
	10.2131	10.3231	10.4295	9.5434	9.6841	9.8188	8.9353	9.1110	9.2769	8.3286	8.5487	8.7528
	13.5621	13.6531	13.7420	12.1046	12.2344	12.3599	11.0090	11.1817	11.3463	10.0440	10.2700	10.4815
	16.5149	16.6020	16.6873	14.1240	14.2551	14.3820	12.5798	12.7584	12.9290	11.3264	11.5643	11.7873
60	2.8590	3.0795	3.2585	2.8560	3.0799	3.2612	2.8492	3.0777	3.2621	2.8395	3.0745	3.2632
	6.6357	6.7890	6.9324	6.5550	6.7173	6.8685	6.4535	6.6271	6.7879	6.3233	6.5122	6.6858
	10.3620	10.4698	10.5743	10.0351	10.1571	10.2749	9.6807	9.8199	9.9533	9.2729	9.4346	9.5884
	13.9889	14.0722	14.1540	13.1971	13.2993	13.3992	12.4471	12.5714	12.6920	11.6736	11.8264	11.9735
	17.4645	17.5340	17.6026	15.9905	16.0830	16.1738	14.7665	14.8851	15.0008	13.6179	13.7698	13.9167
80	2.8596	3.0801	3.2591	2.8588	3.0812	3.2615	2.8551	3.0801	3.2621	2.8497	3.0783	3.2628
	6.6465	6.8000	6.9435	6.6029	6.7614	6.9092	6.5437	6.7086	6.8620	6.4645	6.6382	6.7992
	10.4100	10.5177	10.6221	10.2226	10.3384	10.4504	10.0012	10.1269	10.2481	9.7265	9.8657	9.9992
	14.1224	14.2049	14.2859	13.6476	13.7410	13.8324	13.1407	13.2471	13.3511	12.5627	12.6866	12.8070
	17.7584	17.8255	17.8918	16.8293	16.9099	16.9894	15.9318	16.0284	16.1232	14.9900	15.1074	15.2221
120	2.8599	3.0805	3.2595	2.8606	3.0818	3.2613	2.8592	3.0816	3.2619	2.8570	3.0809	3.2623
	6.6541	6.8077	6.9513	6.6369	6.7926	6.9381	6.6106	6.7691	6.9171	6.5735	6.7361	6.8875
	10.4428	10.5506	10.6551	10.3609	10.4722	10.5801	10.2553	10.3711	10.4833	10.1146	10.2367	10.3547
	14.2118	14.2941	14.3751	13.9941	14.0813	14.1669	13.7345	13.8278	13.9193	13.4062	13.5079	13.6073
	17.9513	18.0178	18.0835	17.5067	17.5794	17.6512	17.0100	17.0902	17.1693	16.4159	16.5063	16.5953

Table 10
The first five dimensionless frequencies of a DWCNT with CF boundary conditions for various values of slenderness ratio, small-scale parameter, and initially axial force.

λ_1	$e_0a = 0$ nm			$e_0a = 1$ nm			$e_0a = 1.5$ nm			$e_0a = 2$ nm		
	$\overline{N}_{b_i} = 0$	$\overline{N}_{b_i} = 10$	$\overline{N}_{b_i} = 20$	$\overline{N}_{b_i} = 0$	$\overline{N}_{b_i} = 10$	$\overline{N}_{b_i} = 20$	$\overline{N}_{b_i} = 0$	$\overline{N}_{b_i} = 10$	$\overline{N}_{b_i} = 20$	$\overline{N}_{b_i} = 0$	$\overline{N}_{b_i} = 10$	$\overline{N}_{b_i} = 20$
40	2.2556	2.7640	3.0553	2.2581	2.7695	3.0624	2.2593	2.7747	3.0697	2.2610	2.7820	3.0801
	5.5961	5.9060	6.1682	5.5074	5.8317	6.1033	5.4002	5.7425	6.0259	5.2634	5.6302	5.9296
	9.2184	9.3874	9.5472	8.7764	8.9710	9.1528	8.3405	8.5656	8.7730	7.8760	8.1408	8.3807
	12.5845	12.7061	12.8238	11.4696	11.6265	11.7765	10.5607	10.7580	10.9441	9.7166	9.9654	10.1958
	15.6060	15.7113	15.8137	13.6151	13.7611	13.9017	12.2406	12.4329	12.6154	11.0872	11.3379	11.5715
60	2.2575	2.7662	3.0577	2.2594	2.7694	3.0616	2.2600	2.7718	3.0649	2.2608	2.7750	3.0695
	5.6295	5.9402	6.2032	5.5910	5.9080	6.1752	5.5403	5.8654	6.1379	5.4722	5.8086	6.0885
	9.3582	9.5263	9.6856	9.1464	9.3262	9.4956	8.9064	9.1005	9.2822	8.6165	8.8301	9.0283
	12.9673	13.0828	13.1952	12.3784	12.5107	12.6387	11.7905	11.9430	12.0895	11.1549	11.3340	11.5047
	16.4379	16.5271	16.6147	15.2553	15.3656	15.4734	14.2182	14.3533	14.4844	13.2057	13.3729	13.5338
80	2.2581	2.7670	3.0585	2.2598	2.7693	3.0612	2.2602	2.7707	3.0632	2.2607	2.7725	3.0658
	5.6411	5.9521	6.2155	5.6206	5.9352	6.2009	5.5917	5.9107	6.1794	5.5518	5.8772	6.1502
	9.4059	9.5743	9.7339	9.2851	9.4600	9.6253	9.1388	9.3219	9.4944	8.9513	9.1457	9.3279
	13.0956	13.2106	13.3226	12.7451	12.8697	12.9907	12.3588	12.4952	12.6270	11.9021	12.0544	12.2009
	16.7128	16.8000	16.8858	15.9755	16.0751	16.1728	15.2363	15.3507	15.4625	14.4329	14.5670	14.6974
120	2.2586	2.7675	3.0591	2.2599	2.7690	3.0608	2.2603	2.7698	3.0618	2.2606	2.7707	3.0630
	5.6494	5.9607	6.2243	5.6415	5.9543	6.2190	5.6289	5.9437	6.2097	5.6108	5.9285	6.1963
	9.4395	9.6082	9.7682	9.3867	9.5583	9.7208	9.3182	9.4935	9.6592	9.2255	9.4059	9.5761
	13.1846	13.2997	13.4119	13.0242	13.1436	13.2598	12.8310	12.9558	13.0770	12.5818	12.7140	12.8421
	16.9009	16.9877	17.0733	16.5499	16.6424	16.7333	16.1515	16.2509	16.3484	15.6640	15.7729	15.8794

parameter; however, for a lengthy DWCNT with CC boundary conditions (i.e., $\lambda_1 = 120$), the first dimensionless frequency trivially increases with the small-scale parameter. Additionally, excluding the first natural frequency, the natural frequencies of the DWCNT with CC boundary conditions always decrease as the small-scale parameter increases. Based on the presented results in Tables 5–7, the frequencies of a DWCNT with SC boundary conditions are generally between those of a DWCNT with SS and those of that with CC boundary conditions. For a DWCNT with SC boundary conditions subjected to initially axial forces (see Table 7), all the dimensionless frequencies decrease with the small-scale parameter. In the case of a DWCNT with S_fS boundary conditions (see Table 8), variation of the small-scale effect parameter has a trivial effect on the variation of dimensionless natural frequencies. For a DWCNT subjected to a particular value of initially axial force, variation of the

slenderness ratio has a slight effect on the variation of dimensionless natural frequencies of the DWCNT with lower mode numbers. Regarding DWCNTs with S_fC boundary conditions (see Table 9), for a specified value of the slenderness ratio, the first dimensionless natural frequency commonly increases with the small-scale parameter. However, the rate of change of the first dimensionless frequency as a function of the small-scale parameter decreases with the slenderness ratio of the DWCNT. As it is seen in Table 8, for a lengthy DWCNT with S_fC boundary conditions (i.e., $\lambda_1 = 120$), the variation of the small-scale parameter has a trivial effect on the variation of the first dimensionless flexural frequency of the DWCNT. In such a case, the effect of variation of the initially axial force on the variation of the first natural frequency is more obvious with respect to other frequencies. It is also clear from Table 8 that excluding the frequency corresponding to the first mode of vibration, the frequencies of other vibration modes decrease with the small-scale parameter. Concerning the free vibration of a DWCNT with CF boundary conditions (see Table 10), the first dimensionless flexural frequency increases with the small-scale parameter for all levels of the slenderness ratio. For a lengthy DWCNT, similar to the previously studied boundary conditions, the variation of the small-scale parameter has a trivial effect on the variation of the first dimensionless flexural frequency of the DWCNT. A brief scrutiny of the presented results in Tables 5–10 also reveals that the variation of the initially axial force within the DWCNT with CF conditions is most influential on the first dimensionless flexural frequency with respect to other boundary conditions.

5.3. Vibration modes patterns of the innermost and outermost tubes of the DWCNT under different conditions

In this part, the vibrational mode shapes associated with the natural frequencies of the DWCNT are plotted for different boundary conditions. It is emphasized herein that the effect of influential parameters on the vibration mode patterns of the lengthy DWCNT as well as the amplitude ratio between the innermost and outermost tubes are not of concern. However, the focal focus of the author is on the general patterns of the flexural vibration modes of the innermost and outermost tubes of the DWCNT under different conditions. For this purpose, the first ten vibration mode shapes of the DWCNT are demonstrated in Figs. 3–8 for various boundary conditions. The plotted results are provided for freely vibrant DWCNTs with $\lambda_1 = 40$ and $\mu = 0$ when no initially axial forces are exerted on DWCNTs (i.e., K_r=K_t=N_{b_i}=0). In these figures, the mode shapes pertinent to the innermost and the outermost tubes have been shown by the solid lines and the dotted lines, respectively.

In Fig. 3, the predicted vibration modes of the DWCNT with SS boundary conditions and their correspondence dimensionless flexural frequencies are given. As it is clear, the dynamic amplitudes of the innermost tube are generally greater than those of the outermost tube. In the cases of the first four modes of vibration, the DWCNT commonly exhibits a coaxial vibration pattern and the dynamic amplitudes of the innermost and outermost tubes are approximately the same. For the fifth mode of vibration, the noncoaxial deflections of the innermost and outermost tubes of the DWCNT are apparent. The second, third, fourth, fifth, and tenth modes of vibration of the DWCNT in order consist of two, three, four, five, and six half-waves and the deflections of the innermost and outermost tubes are in the same direction. For the cases of the sixth to the ninth vibration modes, obvious noncoaxial vibration modes are predicted by the proposed model. The sixth, seventh, eighth, and ninth vibration modes are composed of two, one, three, and four half-waves of vibration, respectively. For these vibration modes, the deflections of the innermost tube are in the opposite direction of those of the outermost tube.

The first ten vibration mode shapes of the DWCNT with CC conditions as well as the values of the corresponding dimensionless flexural frequencies are illustrated in Fig. 4. The first three vibration modes show somewhat coaxial vibration modes such that the dynamic amplitudes of deflection of the innermost tube are fairly greater than those of the outermost tube. The

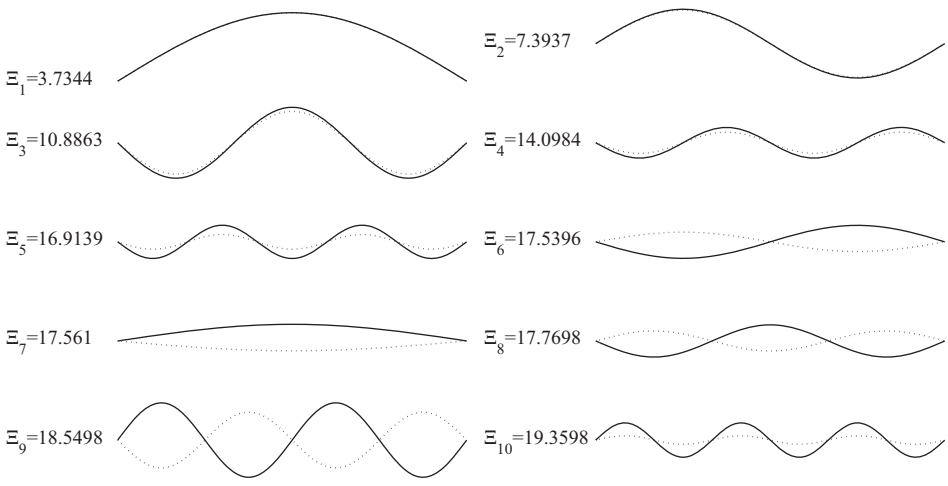

Fig. 3. The first ten transverse vibration modes of the innermost and outermost tubes of a DWCNT with SS boundary conditions ($\lambda_1 = 40$, $e_0a = 0$; (...) outermost tube, (—) innermost tube).

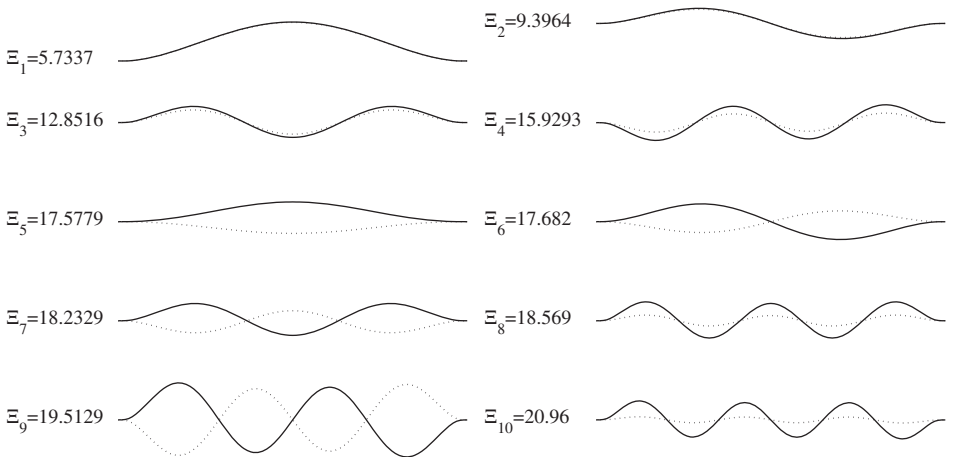

Fig. 4. The first ten transverse vibration modes of the innermost and outermost tubes of a DWCNT with CC boundary conditions ($\lambda_1 = 40$, $e_0a = 0$; $K_{t_i} = K_{r_i} = N_{b_i} = 0$; (...) outermost tube, (—) innermost tube).

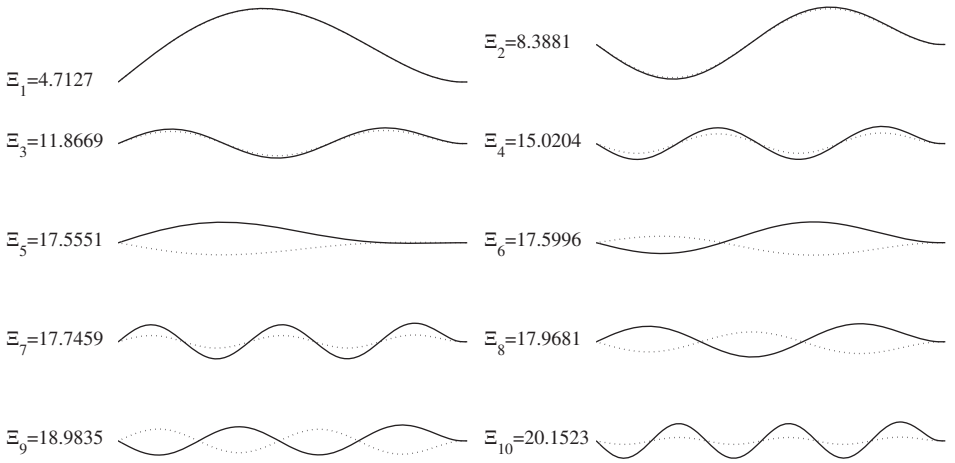

Fig. 5. The first ten transverse vibration modes of the innermost and outermost tubes of a DWCNT with SC boundary conditions ($\lambda_1 = 40$, $e_0a = 0$; $K_{t_i} = K_{r_i} = N_{b_i} = 0$; (...) outermost tube, (—) innermost tube).

fifth, sixth, seventh, and ninth vibration modes of the DWCNT have been consisted of one, two, three, and four half-waves, respectively. In such vibration modes, the deflections of the outermost tube are in the opposite direction with respect to those of the innermost tube. The eighth and tenth modes of vibration are, respectively, characterized by five and six half-waves and the innermost and outermost tubes have been deflected in the same direction. For these vibration modes, the dynamic amplitude deflections of the innermost are also greater than those of the outermost tube.

Fig. 5 shows the first ten vibration modes of the DWCNT with SC boundary conditions. As it is seen in Fig. 5, the first three modes of vibration of the DWCNT are approximately coaxial since the deflections of both the innermost and outermost tubes are the same and the amplitudes of the vibration modes of both the inner and outer tubes are fairly similar. The fifth, sixth, eighth, and ninth modes of vibration consist of one, two, three, and four half-waves and the deflections of the innermost and outermost tubes are in the opposite direction.

The first ten vibration modes as well as their pertinent dimensionless frequency values of the DWCNT under S_fS conditions are provided in Fig. 6. The first three vibration modes exhibit the coaxial vibration pattern. The first, second, third, fourth, fifth, and tenth vibration modes are consisting of one, three, five, seven, nine, and eleven quarter-waves, respectively, and the deflections of the innermost and outermost tubes are in the same direction. The sixth, seventh, eighth, and ninth vibration modes have, respectively, three, one, five, and seven quarter-waves and they are clearly noncoaxial. In such vibration modes, the deflections of the innermost and outermost tubes are in the opposite direction as well.

In Fig. 7, the first ten vibration modes of the innermost and outermost tubes of the DWCNT with S_fC boundary conditions as well as the values of the corresponding dimensionless flexural frequencies are presented. A brief comparison between the

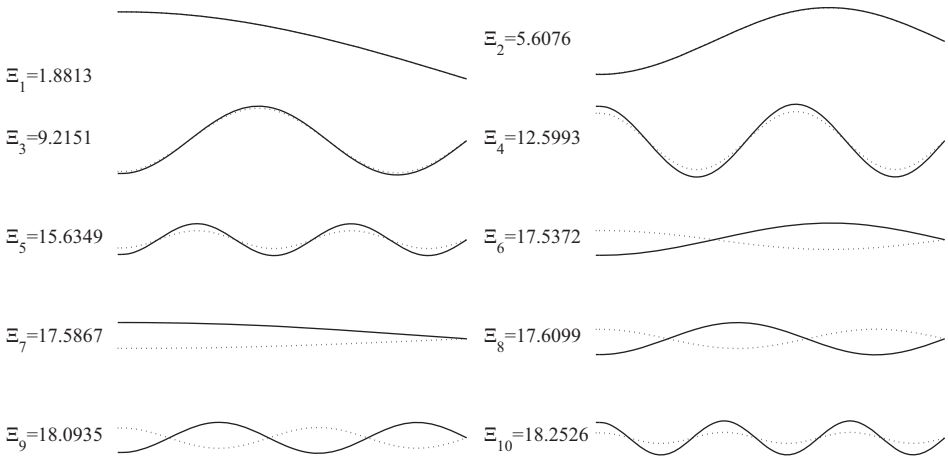

Fig. 6. The first ten transverse vibration modes of the innermost and outermost tubes of a DWCNT with S_fS boundary conditions ($\lambda_1 = 40$, $e_0a = 0$; $K_{t_i} = K_{r_i} = N_{b_i} = 0$; (...) outermost tube, (—) innermost tube).

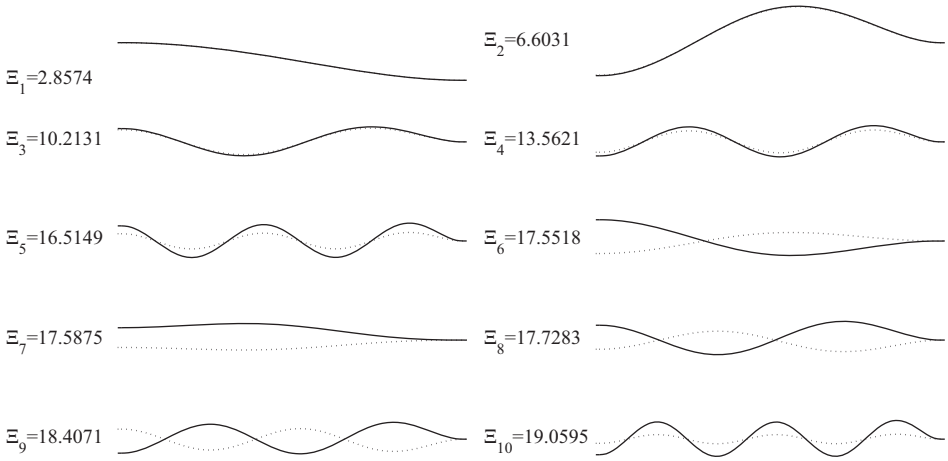

Fig. 7. The first ten transverse vibration modes of the innermost and outermost tubes of a DWCNT with S_fC boundary conditions ($\lambda_1 = 40$, $e_0a = 0$; $K_{t_i} = K_{r_i} = N_{b_i} = 0$; (...) outermost tube, (—) innermost tube).

plotted vibration modes in Figs. 6 and 7 indicates that the patterns of vibration modes of the DWCNT with S_fC conditions are somehow similar to the case of the DWCNT under S_fS conditions.

Finally, the first ten vibration modes of the DWCNT with CF boundary conditions as well as the values of their corresponding dimensionless frequencies are provided in Fig. 8. The first four modes display coaxial vibration pattern. Moreover, in the fifth and tenth modes of vibration modes, the deflection amplitudes of the innermost tube are apparently larger than those of the outermost tube. For the sixth, seventh, eighth, and ninth modes of vibration, there exists noncoaxial vibration patterns. In such cases, the deflections of the tubes are in the opposite direction. Additionally, the amplitudes of deflections of the innermost tube are somewhat greater than those of the outermost tube.

5.4. Parametric studies

In this part, the effects of the slenderness ratio of the innermost tube, small-scale parameter, initially axial force, lateral and rotational stiffness of the surrounding matrix on the first five flexural frequencies of DWCNTs are investigated for different boundary conditions. The radii of the innermost and outermost tubes are considered as $r_{m_1} = 3$ nm and $r_{m_2} = 3.34$ nm, respectively.

5.4.1. Effect of slenderness ratio on the natural frequencies of DWCNTs

The effects of the slenderness ratio of the innermost tube on the dimensionless flexural frequencies of a DWCNT with different boundary conditions are of concern. In the absence of the initially axial force, a freely excitable DWCNT is considered

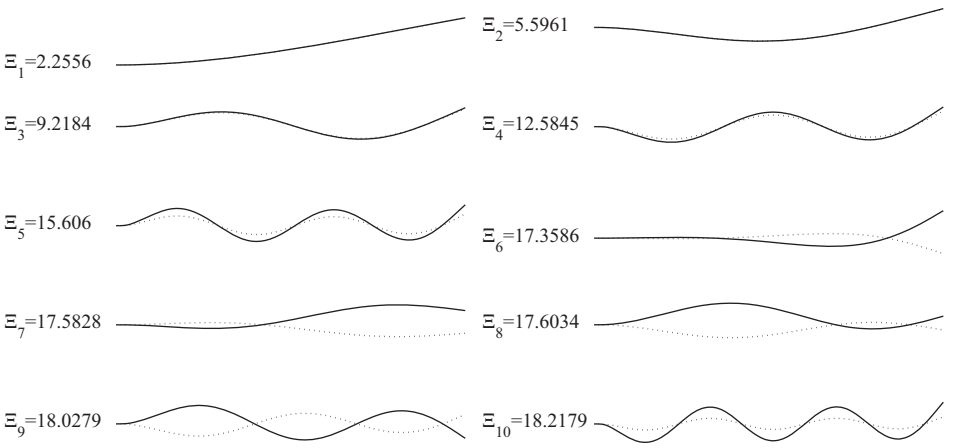

Fig. 8. The first ten transverse vibration modes of the innermost and outermost tubes of a DWCNT with CF boundary conditions ($\lambda_1 = 40$, $e_0a = 0$; $K_{t_i} = K_{r_i} = N_{b_i} = 0$; (...) outermost tube, (—) innermost tube).

(i.e., $\overline{K}_t = \overline{K}_r = \overline{N}_{b_i} = 0$). The plots of the first dimensionless natural frequencies in terms of the slenderness ratio of the innermost tube have been provided for the understudy DWCNT with SS, CC, SC, and CF boundary conditions in Fig. 9(a), (b), (c), and (d), respectively. The predicted results have been given for three levels of the small-scale parameter (i.e., $e_0a = 0$, 1, and 2 nm). As it is obvious in Fig. 9(a)–(d), the dimensionless frequencies of the DWCNT for each boundary conditions increase with the slenderness ratio such that the dimensionless frequency of each mode would converge to a specific value, irrespective of the small-scale parameter. It implies that for higher levels of the slenderness ratio, the variation of the small-scale parameter has a trivial effect on the variation of dimensionless natural frequencies. For all boundary conditions, the variation of the small-scale effect parameter is more influential on the frequencies of higher modes of vibration.

5.4.2. Effect of small-scale parameter on the natural frequencies of DWCNTs

In Fig. 10(a)–(d), the first five dimensionless natural frequencies of a DWCNT with $\lambda_1 = 20$ as a function of the small-scale parameter have been plotted for different boundary conditions. The results are presented in the absence of initially axial force when the DWCNT has been released from the surrounding matrix. As it is seen in Fig. 10(a)–(d), the natural frequencies generally decrease with the small-scale parameter, irrespective of the boundary conditions of the DWCNT. This matter is more obvious for the frequencies corresponding to the higher modes of vibration. A scrutiny of the plotted results in

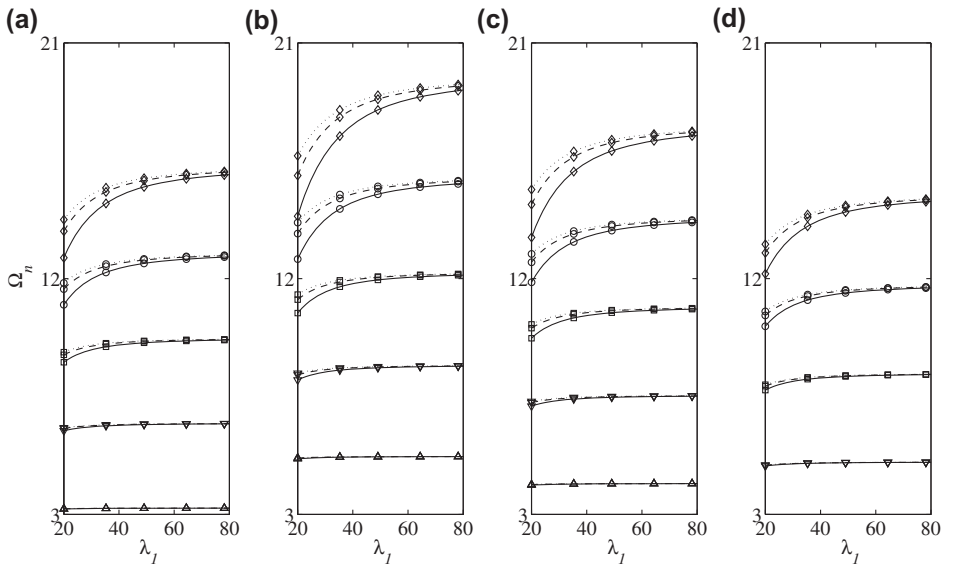

Fig. 9. Variation of the first five nondimensional frequencies of the DWCNT in terms of slenderness ratio for different values of small-scale parameter: (a) SS, (b) CC, (c) SC, (d) CF; ((...) $e_0a = 0$ (nm), (–.–) $e_0a = 1$ (nm), (—) $e_0a = 2$ (nm); (△) Ω_1, (▽) Ω_2, (□) Ω_3, (○) Ω_4, (◇) Ω_5; $K_{t_i} = K_{r_i} = N_{b_i} = 0$).

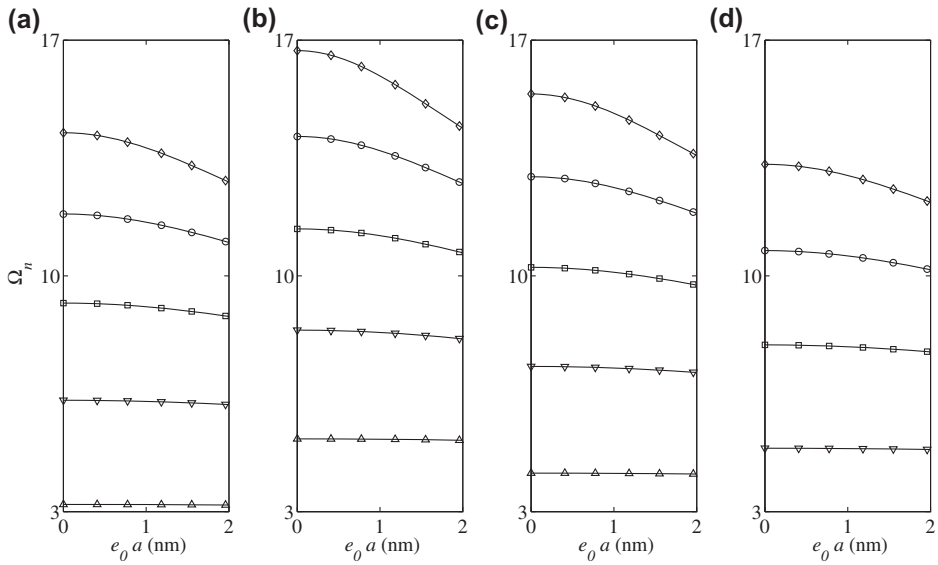

Fig. 10. Variation of the first five nondimensional frequencies of the DWCNT in terms of small-scale parameter: (a) SS, (b) CC, (c) SC, (d) CF; ((△) Ω_1, (▽) Ω_2, (□) Ω_3, (○) Ω_4, (◇) Ω_5; $\lambda_1 = 20; K_{t_i} = K_{r_i} = N_{b_i} = 0$).

Fig. 10(a)–(d) is also indicated that the influence of the small-scale parameter on the natural frequencies is, respectively, less and more noticeable to the DWCNTs with CF and CC conditions with respect to other cases.

5.4.3. Effect of lateral stiffness of the surrounding matrix on the natural frequencies of DWCNTs

In this part, the influence of lateral stiffness of the surrounding matrix on the natural frequencies of the DWCNT embedded in an elastic medium is of particular interest. For this purpose, the first five dimensionless frequencies of the DWCNT as a function of the dimensionless lateral stiffness of the surrounding matrix are provided in Fig. 11(a)–(d) for different boundary conditions as well as small-scale parameters. The slenderness ratio of the innermost tube is set equal to 20. It is assumed that the surrounding matrix does not resist against rotation of the DWCNT (i.e., $K_r = 0$), and both the innermost and outermost tubes do not experience initially axial forces. As it is obvious from the presented results in Fig. 11(a)–(d), the natural frequencies of the DWCNT increase with the lateral stiffness of the surrounding matrix for all boundary conditions. Furthermore, the

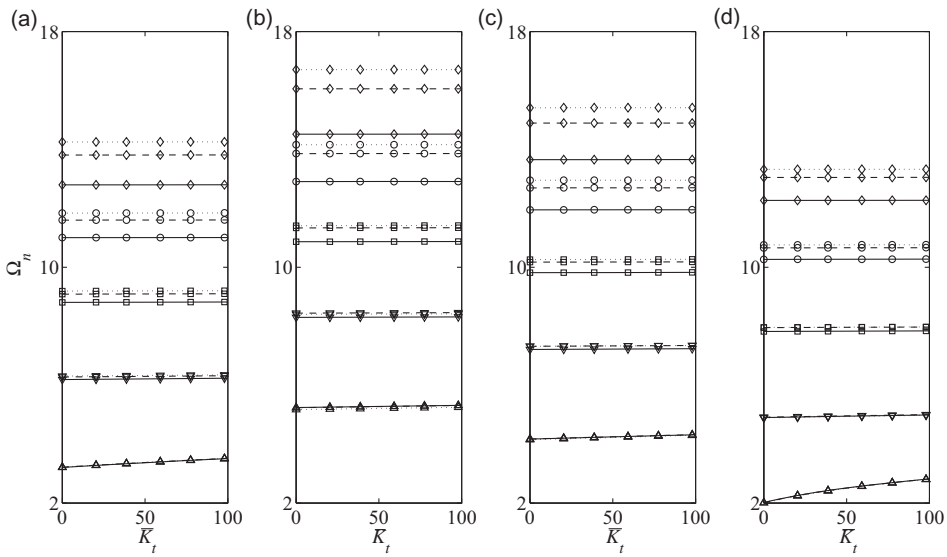

Fig. 11. Variation of the first five nondimensional frequencies of the DWCNT in terms of dimensionless lateral stiffness of the surrounding matrix for different values of small-scale parameter: (a) SS, (b) CC, (c) SC, (d) CF; ((. . .) $e_0a = 0$ (nm), (−.−) $e_0a = 1$ (nm), (−) $e_0a = 2$ (nm); (△) Ω_1, (▽) Ω_2, (□) Ω_3, (○) Ω_4, (◇) Ω_5; $\lambda_1 = 20; K_{r_i} = N_{b_i} = 0$).

variation of the lateral stiffness of the surrounding matrix is more influential on the variation of the dimensionless natural frequencies of the lower modes of vibration. A brief survey of the plotted results in Fig. 11(a)–(d) shows that the variation of the lateral stiffness of the surrounding medium has the most influence on the variation of the first natural frequency of the DWCNT with CF boundary conditions in compare to other cases. However, the effect of the lateral stiffness on the first natural frequency of the DWCNT with CC boundary conditions is very trivial. For an assumed value of the lateral stiffness of the surrounding matrix, the predicted dimensionless natural frequencies would lessen with the small-scale parameter, irrespective of the boundary condition of the DWCNT. The plotted results in Fig. 11(a)–(d) indicate that the rate of decreasing of the frequencies due to the variation of the small-scale parameter is more apparent to those frequencies associated with the higher modes of vibration.

5.4.4. Effect of rotational stiffness of the surrounding matrix on the natural frequencies of DWCNTs

Herein, the effect of the rotational stiffness of the surrounding medium of the DWCNT on the first five dimensionless natural frequencies of the DWCNT is of concern. Consider a DWCNT with the innermost tube's slenderness ratio equal to 20 and its both tubes are free from any initial axial force. Since the effect of only rotational stiffness of the surrounding matrix on the vibration characteristics of the DWCNT is of interest, the lateral stiffness of the surrounding matrix is set equal to zero. The plotted results in Fig. 12(a)–(d) have been provided for various boundary conditions as well as different levels of the small-scale parameter. The obtained results reveal that an increase in the rotational stiffness of the surrounding matrix leads to an increase of the first dimensionless frequency of the DWCNT, irrespective of the small-scale effect parameter and the boundary condition of the DWCNT. Except the CF boundary condition, there exists roughly a linear relationship between the predicted dimensionless frequencies and the dimensionless rotational stiffness of the surrounding matrix (see Fig. 12(a)–(c)). According to the graphically presented results in Fig. 12(a)–(d), the effect of the variation of the rotational stiffness constant on the frequencies of the lower vibration's modes is more obvious with respect to those of higher vibration's modes. The demonstrated results in Fig. 12(a)–(d) also reveal that the variation of the rotational stiffness of the surrounding matrix has the most influence on the variation of first natural frequency of the DWCNT with CF boundary conditions. This matter follows with lower rate as one moves from CF to SS, then SC, and finally CC boundary conditions.

5.4.5. Effect of initially axial force on the natural frequencies of DWCNTs

Another interesting parametric study is carried out to determine the effect of the initially axial forces within the innermost and outermost tubes on the natural frequencies of the DWCNT. To this end, an elastically supported DWCNT with slenderness ratio of the innermost tube equal to 20 which has been released from the surrounding matrix is considered. The plots of the first five dimensionless frequencies as a function of dimensionless initially axial forces within the nanotubes of the DWCNT are presented in Fig. 13(a)–(d) for different boundary conditions as well as various values of small-scale parameters. According to the plotted results in Fig. 13(a)–(d), for all considered boundary conditions, the dimensionless natural frequencies increase with the dimensionless initially axial force. Moreover, the influence of the initially axial force on the lower natural frequencies of the DWCNT is more apparent. For a DWCNT with assumed values of initially axial forces, the natural

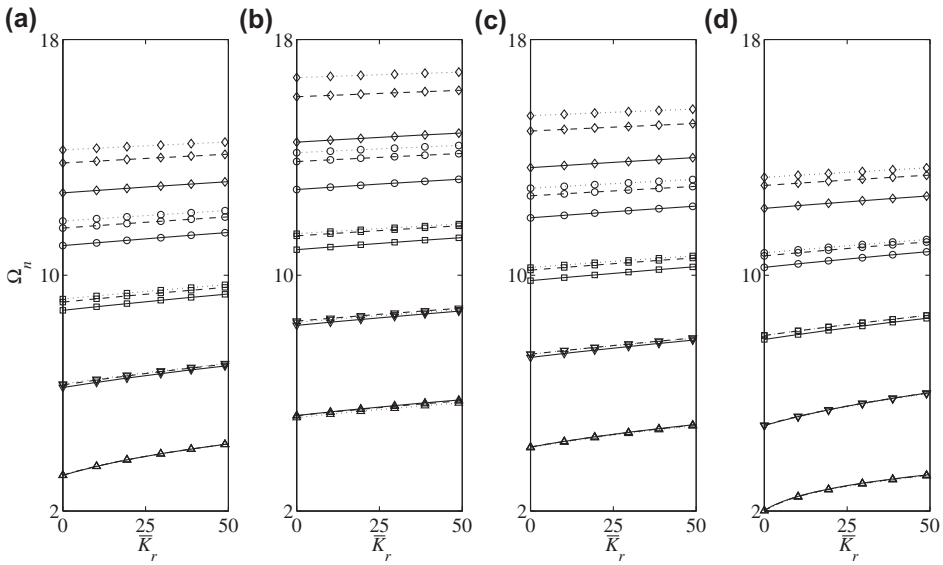

Fig. 12. Variation of the first five nondimensional frequencies of the DWCNT in terms of dimensionless rotational stiffness of the surrounding matrix for different values of small-scale parameter: (a) SS, (b) CC, (c) SC, (d) CF; ((...) e_0a = 0 (nm), (−.−) e_0a=1 (nm), (−) e_0a = 2 (nm); (△) Ω_1, (▽) Ω_2, (□) Ω_3, (○) Ω_4, (◇) Ω_5; $\lambda_1 = 20; K_{t_i} = N_{b_i} = 0$).

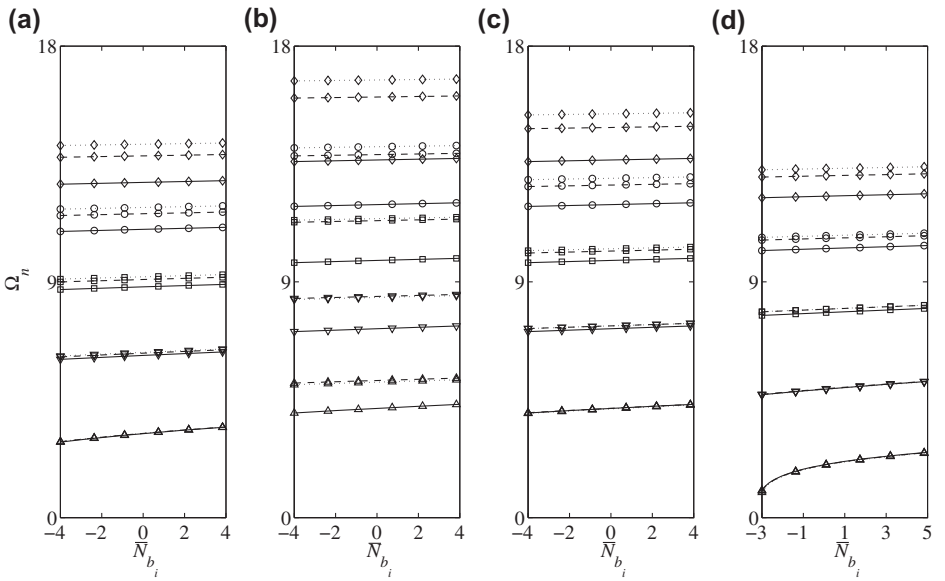

Fig. 13. Variation of the first five nondimensional frequencies of the DWCNT in terms of dimensionless initially axial force for different values of small-scale parameter: (a) SS, (b) CC, (c) SC, (d) CF; ((...) $e_0a = 0$ (nm), (−.−) $e_0a = 1$ (nm), (—) $e_0a = 2$ (nm); (△) Ω_1, (▽) Ω_2, (□) Ω_3, (○) Ω_4, (◇) Ω_5; $\lambda_1 = 20$; $K_{t_i} = K_{r_i} = 0$).

frequencies would lessen as the small-scale parameter becomes highlighted; however, this fact is more obvious for the natural frequencies of higher modes of vibration. For the studied range of the initially axial forces, the variation of the initially axial forces has the less/most effect on the variation of the natural frequencies of the DWCNT with CC/CF boundary conditions with respect to other cases.

6. Conclusions

For different boundary conditions, free transverse dynamic responses of lengthy double-walled carbon nanotubes (DWCNTs) embedded in an elastic matrix are examined in the context of the nonlocal continuum theory of Eringen. To this end, the equivalent continuum structures (ECSs) associated with the innermost and outermost tubes are considered. The interaction van der Waals forces between the atoms of the innermost and outermost tubes are modeled via a continuous lateral spring connecting two tubes. The interaction of the DWCNT with its surrounding medium is is also simulated by continuous lateral and rotary springs, which are attached to the outer ECS through its length. The two attached lengthy ECSs are then modeled by using nonlocal Rayleigh beam theory. The dimensionless equations of motion describing free transverse vibrations of the elastically supported DWCNT embedded in an elastic medium are derived. Finding an analytical solution to the obtained governing equations with their general boundary conditions is a very difficult job. Such solutions are available for some special cases. To bridge such a scientific gap, reproducing kernel particle method (RKPM) is proposed as an alternative efficient scheme. The deflection fields of the innermost and outermost tubes, the only unknowns of the problem, are discretized using appropriate shape functions of RKPM. By introducing appropriate test functions to the governing equations and using integration by parts, the set of algebraic equations describing motion of the considered DWCNT are obtained. For a lengthy DWCNT with different boundary conditions, the eigenvalues and eigenvectors of the set of eigenvalue equations are calculated. In some special cases, the obtained results are also compared with those of other researchers and a reasonably good agreement is achieved. The effects of the slenderness ratio, small-scale parameter, lateral and rotational stiffness of the surrounding matrix, and initially axial force on the first five dimensionless flexural frequencies of the DWCNT embedded in an elastic matrix are explored for different boundary conditions via comprehensive parametric studies. The roles of the influential parameters on the free variation of DWCNTs under different boundary conditions are also displayed and discussed in some detail.

References

[1] H.W. Kroto, J.R. Heath, S.C. ÖBrien, R.F. Curl, R.E. Smalley, C60 Buckyminsterfullerence, Nature 318 (1985) 162–165.
[2] S. Iijima, T. Icihashi, Single-shell carbon nanotubes of 1-nm diameter, Nature 363 (1993) 603–605.
[3] D.S. Bethune, C.H. Kiang, M.S. de Vries, G. Gorman, R. Savoy, J. Vazquez, R. Beyers, Cobalt-catalysed growth of carbon nanotubes with single-atomic-layer walls, Nature 363 (1993) 605–607.
[4] M.M.J. Treacy, T.W. Ebbesen, T.M. Gibson, Exceptionally high Young's modulus observed for individual nanotubes, Nature 381 (1996) 678.
[5] E.W. Wong, P.E. Sheehan, C.M. Lieber, Nanobeam mechanics: elasticity, strength, and toughness of nanorods and nanotubes, Science 277 (1997) 1971.

[6] M.R. Falvo, G.J. Clary, R.M. Taylor, V. Chi, F.P. Brooks, S. Washburn, Bending and buckling of carbon nanotubes under large strain, Nature 389 (1997) 582.
[7] C. Bower, R. Rosen, L. Jin, J. Han, O. Zhou, Deformation of carbon nanotubes in nanotubepolymer composites, Appl. Phys. Lett. 74 (1999) 3317.
[8] C. Dekker, Carbon nanotubes as molecular quantum wires, Phys. Today 52 (1999) 22.
[9] E.T. Thostenson, T. Chou, On the elastic properties of carbon nanotube-based composites: Modeling and characterization, J. Phys. D: Appl. Phys. 36 (2003) 573–582.
[10] Q. Zheng, Q. Jiang, Multiwalled carbon nanotubes as gigahertz oscillators, Phys. Rev. Lett. 88 (4) (2002) 045503 (1-3).
[11] Q. Zheng, J.Z. Liu, Q. Jiang, Excess van der Waals interaction energy of a multiwalled carbon nanotube with an extruded core and the induced core oscillation, Phys. Rev. B 65 (24) (2002) 245409 (1-6).
[12] C. Li, T.W. Chou, Single-walled nanotubes as ultrahigh frequency nanomechanical resonators, Phys. Rev. B 68 (2003) 073405 (1-4).
[13] J. Yoon, C.Q. Ru, A. Mioduchowski, Noncoaxial resonance of an isolated multiwall carbon nanotube, Phys. Rev. B 66 (2002) 233401 (1-4).
[14] J. Yoon, C.Q. Ru, A. Mioduchowski, Vibrations of an embedded multiwall carbon nanotube, Compos. Sci. Technol. 63 (2003) 1533–1542.
[15] Y. Zhang, G. Liu, X. Han, Transverse vibrations of double-walled carbon nanotubes under compressive axial load, Phys. Lett. A 340 (2005) 258–266.
[16] C.M. Wang, V.B.C. Tan, Y.Y. Zhang, Timoshenko beam model for vibration analysis of multi-walled carbon nanotubes, J. Sound Vib. 294 (2006) 1060–1072.
[17] A. Pantano, M.C. Boyce, D.M. Parks, Nonlinear structural mechanics based modeling of carbon nanotube deformation, Phys. Rev. Lett. 91 (14) (2003) 145504 (1-4).
[18] A. Pantano, M.C. Boyce, D.M. Parks, Mechanics of deformation of single and multi-wall carbon nanotubes, J. Mech. Phys. Solids 52 (4) (2004) 789–821.
[19] C. Sun, K. Liu, Vibration of multi-walled carbon nanotubes with initial axial loading, Solid State Commun. 143 (2007) 202–207.
[20] T. Natsuki, Q.Q. Ni, M. Endo, Analysis of the vibration characteristics of double-walled carbon nanotubes, Carbon 46 (2008) 1570–1573.
[21] M. Aydogdu, Vibration of smulti-walled carbon nanotubes by generalized shear deformation theory, Int. J Mech. Sci. 50 (2008) 837–844.
[22] M. Aydogdu, Effects of shear deformation on vibration of double-walled carbon nanotubes embedded in an elastic medium, Arch. Appl. Mech. 78 (2008) 711–723.
[23] M.A. Shubov, M.R. Arenaza, Vibrational frequency distribution for nonconservative model of double-walled carbon nanotube, Appl. Math. Comput. 217 (2010) 1246–1252.
[24] N.H. Sweilam, M.M. Khader, Approximate solutions to the nonlinear vibrations of multiwalled carbon nanotubes using Adomian decomposition method, Appl. Math. Comput. 217 (2010) 495–505.
[25] G.D. Mahan, Oscillations of a thin hollow cylinder: Carbon nanotubes, Phys. Rev. B 65 (23) (2002) 235402 (1-7).
[26] K. Dong, X. Wang, Wave propagation in carbon nanotubes embedded in an elastic matrix, Arch. Appl. Mech. 77 (2007) 575–586.
[27] K. Dong, S.Q. Zhu, X. Wang, Wave propagation in multiwall carbon nanotubes embedded in a matrix material, Compos. Struct. 82 (2008) 1–9.
[28] E. Cosserat, F. Cosserat, Theorie des Corps Deformables, Hermann et Fils, Paris, 1909.
[29] R.A. Toupin, Elastic materials with couple stresses, Arch. Ration. Mech. Anal. 11 (1964) 385–414.
[30] R.D. Mindlin, Micro-structure in linear elasticity, Arch. Ration. Mech. Anal. 16 (1964) 51–78.
[31] A.C. Eringen, On differential equations of nonlocal elasticity and solutions of screw dislocation and surface waves, J. Appl. Phys. 54 (1983) 4703–4710.
[32] A.C. Eringen, Nonlocal Continuum Field Theories, Springer-Verlag, New York, 2002.
[33] E.C. Aifantis, On the role of gradients in the localization of deformation and fracture, Int. J. Eng. Sci. 30 (10) (1992) 1279–1299.
[34] W.H. Duan, C.M. Wang, Y.Y. Zhang, Calibration of nonlocal scaling effect parameter for free vibration of carbon nanotubes by molecular dynamics, J. Appl. Phys. 101 (2007) 024305 (1-7).
[35] Y.Q. Zhang, G.R. Liu, X.Y. Xie, Free transverse vibrations of double-walled carbon nanotubes using a theory of nonlocal elasticity, Phys. Rev. B 71 (2005) 195404 (1-7).
[36] Q. Wang, G.Y. Zhou, K.C. Lin, Scale effect on wave propagation of double-walled carbon nanotubes, Int. J. Solids Struct. 43 (2006) 6071–6084.
[37] Q. Wang, A.K. Varadan, Vibration of carbon nanotubes studied using nonlocal continuum mechanics, Smart Mater. Struct. 15 (2006) 659–666.
[38] P. Lu, H.P. Lee, C. Lu, P.Q. Zhang, Application of nonlocal beam models for carbon nanotubes, Int. J. Solids Struct. 44 (2007) 5289–5300.
[39] M.C. Ece, M. Aydogdu, Nonlocal elasticity effect on vibration of in-plane loaded double-walled carbon nano-tubes, Acta Mech. 190 (2007) 185–195.
[40] X.F. Li, B.L. Wang, Y.W. Mai, Effects of a surrounding elastic medium on flexural waves propagating in carbon nanotubes via nonlocal elasticity, J. Appl. Phys. 103 (2008) 074309 (1-9).
[41] R. Li, G.A. Kardomateas, Vibration characteristics of multiwalled carbon nanotubes embedded in elastic media by a nonlocal elastic shell model, J. Appl. Mech. 74 (2007) 1087–1094.
[42] Y.G. Hu, K.M. Liew, Q. Wang, X.Q. He, B.I. Yakobson, Nonlocal shell model for elastic wave propagation in single- and double-walled carbon nanotubes, J. Mech. Phys. Solids 56 (2008) 3475–3485.
[43] K. Kiani, Application of nonlocal beam models to double-walled carbon nanotubes under a moving nanoparticle. Part I: theoretical formulations, Acta Mech. 216 (2011) 165–195.
[44] K. Kiani, Application of nonlocal beam models to double-walled carbon nanotubes under a moving nanoparticle. Part II: parametric study, Acta Mech. 216 (2011) 197–206.
[45] W.K. Liu, S. Jun, Y.F. Zhang, Reproducing kernel particle methods, Int. J. Numer. Methods Eng. 20 (1995) 1081–1106.
[46] W.K. Liu, S. Jun, S. Li, J. Adee, T. Belytschko, Reproducing kernel particle methods for structural dynamics, Int. J. Numer. Methods Eng. 38 (1995) 1655–1679.
[47] W.K. Liu, Y. Chen, S. Jun, J.S. Chen, T. Belytschko, C. Pan, R.A. Uras, C.T. Chang, Overview and applications of the reproducing kernel particle methods, Arch. Comput. Methods Eng. 3 (1996) 3–80.
[48] K. Kiani, A. Nikkhoo, B. Mehri, Prediction capabilities of classical and shear deformable beam theories excited by a moving mass, J. Sound Vib. 320 (2009) 632–648.
[49] K. Kiani, A. Nikkhoo, On the limitations of linear beams for the problems of moving mass-beam interaction using a meshless method, Acta Mech. Sinica 28 (2011) 164–179.
[50] K. Kiani, A meshless approach for free transverse vibration of embedded single-walled nanotubes with arbitrary boundary conditions accounting for nonlocal effect, Int. J. Mech. Sci. 52 (10) (2010) 1343–1356.
[51] K. Kiani, B. Mehri, Assessment of nanotube structures under a moving nanoparticle using nonlocal beam theories, J. Sound Vib. 329 (11) (2010) 2241–2264.
[52] K. Kiani, Longitudinal and transverse vibration of a single-walled carbon nanotube subjected to a moving nanoparticle accounting for both nonlocal and inertial effects, Physica E 42 (9) (2010) 2391–2401.
[53] J.L. Kuang, A.Y.T. Leung, Chaotic flexural oscillations of a spinning nanoresonator, Nonlinear Dyn. 51 (2008) 9–29.
[54] K. Kiani, Small-scale effect on the vibration of thin nanoplates subjected to a moving nanoparticle via nonlocal continuum theory, J. Sound Vib. 330 (20) (2011) 4896–4914.
[55] K. Kiani, Nonlocal continuum-based modeling of a nanoplate subjected to a moving nanoparticle. Part I: Theoretical formulations, Physica E 44 (1) (2011) 229–248.
[56] K. Kiani, Nonlocal continuum-based modeling of a nanoplate subjected to a moving nanoparticle. Part II: Parametric studies, Physica E 44 (1) (2011) 249–269.
[57] A.G. Arani, M.A. Roudbari, Nonlocal piezoelastic surface effect on the vibration of visco-Pasternak coupled boron nitride nanotube system under a moving nanoparticle, Thin Solid Films 542 (2013) 232–241.

[58] T. Murmu, S.C. Pradhan, Buckling analysis of a single-walled carbon nanotube embedded in an elastic medium based on nonlocal elasticity and Timoshenko beam theory and using DQM, Physica E 41 (7) (2009) 1232–1239.
[59] S. Narendar, S. Gopalakrishnan, Critical buckling temperature of single-walled carbon nanotubes embedded in a one-parameter elastic medium based on nonlocal continuum mechanics, Physica E 43 (6) (2011) 1185–1191.
[60] R. Ansari, M. Hemmatnezhad, Nonlinear vibrations of embedded multi-walled carbon nanotubes using a variational approach, Math. Comput. Modell. 53 (5) (2011) 927–938.
[61] C.W. Lim, On the truth of nanoscale for nanobeams based on nonlocal elastic stress field theory: equilibrium, governing equation and static deflection, Appl. Math. Mech. 31 (1) (2010) 37–54.
[62] C.W. Lim, Y. Yang, Wave propagation in carbon nanotubes: nonlocal elasticity induced stiffness and velocity enhancement effects, J. Mech. Mater. Struct. 5 (3) (2010) 459–476.
[63] Y. Yang, L. Zhang, C.W. Lim, Wave propagation in double-walled carbon nanotubes on a novel analytically nonlocal Timoshenko-beam model, J. Sound Vib. 330 (8) (2011) 1704–1717.
[64] C.W. Lim, Y. Yang, New predictions of size-dependent nanoscale based on nonlocal elasticity for wave propagation in carbon nanotubes, J. Comput. Theor. Nanosci. 7 (6) (2010) 988–995.
[65] K.M. Liu, An introduction to wavelet reproducing kernel particle methods, USACM Bull. 8 (1995) 3–16.
[66] K.M. Liu, Y. Chen, Wavelet and multi-scale reproducing kernel particle methods, Int. J. Numer. Meth. Fluids 21 (1995) 901–931.
[67] L.L. Ke, Y. Xiang, J. Yang, S. Kitipornchai, Nonlinear free vibration of embedded double-walled carbon nanotubes based on nonlocal Timoshenko beam theory, Comput. Mater. Sci. 47 (2009) 409–417.